Cross-Species Analysis Defines the Conservation of Anatomically-Segregated VMH Neuron Populations

Alison H. Affinati[1], Paul V. Sabatini[1], Cadence True[2], Abigail J. Tomlinson[1], Melissa Kirigiti[2], Sarah R. Lindsley[2], Chien Li[3], David P. Olson[4], Paul Kievit[2], Martin G. Myers, Jr.[1]**, and Alan C. Rupp[1]**

[1]Department of Internal Medicine, University of Michigan, Ann Arbor, MI, USA.

[2]Oregon National Primate Research Center, Beaverton, OR, USA.

[3] Novo Nordisk Research Center, Seattle, WA, USA.

[4]Department of Pediatrics, University of Michigan, Ann Arbor, MI, USA

**Correspondence:
Alan C. Rupp, PhD
Martin G Myers, Jr., MD, PhD
Department of Internal Medicine
University of Michigan
2800 Plymouth Rd., Bldg 20
Ann Arbor, MI 48109
Phone: 734-647-9515
Email: ruppa@umich.edu, mgmyers@umich.edu

Conflict of Interest Statement: CL is an employee of Novo Nordisk A/S; the authors have no other competing interests relevant to this manuscript.

ABSTRACT

The ventromedial hypothalamic nucleus (VMH) controls diverse behaviors and physiologic functions, suggesting the existence of multiple VMH neural subtypes with distinct functions. Combing Translating Ribosome Affinity Purification with RNA sequencing (TRAP-seq) data with snRNA-seq data, we identified 24 mouse VMH neuron clusters. Further analysis, including snRNA-seq data from macaque tissue, defined a more tractable VMH parceling scheme consisting of 6 major genetically- and anatomically-differentiated VMH neuron classes with good cross-species conservation. In addition to two major ventrolateral classes, we identified three distinct classes of dorsomedial VMH neurons. Consistent with previously-suggested unique roles for leptin receptor (*Lepr*)-expressing VMH neurons, *Lepr* expression marked a single dorsomedial class. We also identified a class of glutamatergic VMH neurons that resides in the tuberal region, anterolateral to the neuroanatomical core of the VMH. This atlas of conserved VMH neuron populations provides an unbiased starting point for the analysis of VMH circuitry and function.

INTRODUCTION

The ventromedial hypothalamic nucleus (VMH, which primarily contains glutamatergic neurons) plays important roles in a variety of metabolic responses and in the control of behaviors relevant to panic, reproduction, and aggression. The VMH contains several anatomic subdivisions, including the dorsomedial and central VMH (VMH_{DM} and VMH_{C}, respectively, which control autonomic outputs and behavioral responses to emergencies (Lindberg, Chen, and Li 2013; Vander Tuig, Knehans, and Romsos 1982)), and the ventrolateral VMH (VMH_{VL}; known for roles in sexual and social behaviors (Hashikawa et al. 2017; Krause and Ingraham 2017)). The predominantly GABAergic tuberal region of the hypothalamus lies anterolateral to the core of the VMH.

Each VMH subdivision mediates a variety of outputs and thus presumably contains multiple functionally-distinct cell types. For example, activating adult *Nr5a1*-expressing VMH neurons (which includes most cells in the VMH_{DM} and VMH_{C}) promotes panic-related behaviors, augments hepatic glucose output to increase blood glucose, and elevates energy expenditure (Meek et al. 2016, 201; Flak et al. 2020; Kunwar et al. 2015). In contrast, activating the subset of VMH_{DM} cells that expresses leptin receptor (*Lepr*, which encodes the receptor for the adipose-derived, energy balance-controlling hormone, leptin (H. Chen et al. 1996; Tartaglia et al. 1995)) promotes energy expenditure without altering these other parameters (Sabatini et al. 2021; Meek et al. 2013; 2016). Hence, each VMH subregion may contain multiple discrete neuron populations that mediate unique functions.

To date, most analyses of VMH function have utilized *Nr5a1* or candidate markers that do not necessarily align with functionally and/or transcriptionally unique

VMH cell types (Bingham et al. 2006). Thus, to understand VMH-controlled responses, we must use unbiased methods to define discrete subpopulations of VMH neurons, along with markers that permit their selective manipulation. Single-cell approaches (such as single-nucleus RNA-sequencing (snRNA-seq)) can identify neuronal populations in an unbiased manner, and have previously suggested parceling schemes for neurons in many brain areas, including the VMH (D.-W. Kim et al. 2019; Campbell et al. 2017; Habib et al. 2017). Many such analyses define large numbers of highly inter-related cell populations of unclear functional significance and conservation, however (D.-W. Kim et al. 2019; R. Chen et al. 2017; Lam et al. 2017). Determining functions for dozens of cell populations that lie in the same anatomic region and which possess overlapping gene expression profiles (i.e., that don't contain unique marker genes) would represent a daunting task.

In the present study we use Translating Ribosome Affinity Purification with RNA-sequencing (TRAP-seq) in mice together with snRNA-seq of mouse and macaque VMH neurons to define transcriptionally unique, anatomically discrete, conserved, and genetically tractable classes of VMH neurons. These include a distinct *Lepr*-expressing VMH neuron class, along with a set of glutamatergic VMH neurons that resides in the tuberal region. These findings define a starting point for the comprehensive analysis of VMH circuitry and function.

RESULTS

Combining snRNA-seq with *Nr5a1*-directed TRAP-seq defines mouse VMH neuron populations

To define neuronal populations within the mouse VMH in an unbiased manner, we microdissected the VMH of mice and subjected 10 individual tissue samples to snRNA-seq using the 10x Genomics platform (Figure 1A), collecting a total of 42,040 nuclei that passed quality control (Figure 1- figure supplement 1 A–C). The recovered nuclei included all major CNS cell types (Figure 1- figure supplement 1, see Methods for clustering and cell type identification details), including 21,585 neurons that comprised 37 distinct neuronal populations (Figure 1B, C).

Many adult VMH neurons express *Nr5a1* (which encodes the transcription factor, SF1 (Cheung et al. 2013)) and/or *Fezf1* (Kurrasch et al. 2007), whose detection was restricted to a confined cluster of neurons in UMAP space (Figure 1D). Although essentially all VMH neurons express *Nr5a1* during development, only a subset of VMH cells express *Nr5a1* and/or *Fezf1* in adult animals (Cheung et al. 2013; Kurrasch et al. 2007). Furthermore, the inherent noise in snRNA-seq data risks false positives and negatives when using only one or two genes for cell-type identification. To ensure that we identified all VMH cell groups for our analysis, we performed TRAP-seq using *Nr5a1-Cre*;*Rosa26*$^{eGFP\text{-}L10a}$ mice, in which the early developmental expression of *Nr5a1-Cre* promotes the permanent expression of tagged ribosomes across the VMH (Figure 1E). TRAP-seq identified 4,492 transcripts significantly enriched in cells marked by the developmental expression of *Nr5a1*, including *Nr5a1* and *Fezf1* (Figure 1F, Supplementary File 1). Applying this broader VMH-enriched transcriptome to our

snRNA-seq clusters revealed 6 populations of neurons (clusters 6–11; corresponding to the populations with highest *Nr5a1* and *Fezf1* expression) that contain VMH neurons. (Figure 1G,H). Importantly, *Nr5a1*-negative cells (clusters 6 and 7) were identified as VMH by their enrichment of *Nr5a1-Cre* TRAP-seq genes (Figure 1H), suggesting they were developmentally labeled by *Nr5a1-Cre*; these cells presumably reside in the VMH_{VL} (which expresses *Nr5a1* during development, but not in adulthood).

To compare TRAP-seq and snRNA-seq results, we performed “pseudo-TRAP” on pseudobulk samples of our snRNA-seq data, aggregated by cell type (i.e., VMH clusters vs. non-VMH clusters; see Supplementary File 2 for enrichment results). While many genes were enriched in both datasets (1,977), more were specific to one method (Figure 1I, 2,354 genes specific to TRAP and 2,828 specific to pseudo-TRAP). Notably, enrichment was largely a function of expression level: the genes that were enriched in both datasets were highly expressed in both, while the genes that were specific to TRAP or pseudo-TRAP were highly expressed in their enriched dataset, but expressed at lower levels in the other (Figure 1J). This suggests that the two methods may illuminate partially distinct aspects of the transcriptome—TRAP-seq for ribosome-associated genes and snRNA-seq for nuclear-enriched and nascent transcripts—and that their combined use provides a more comprehensive view of cellular state. Finally, many of the genes enriched in both datasets were limited to one or a few populations, highlighting the heterogeneity of gene expression across VMH cell types, even for prominent VMH marker genes (Figure 1K).

To understand the landscape of mouse VMH neuron populations in more detail, we subjected the VMH neurons in clusters 6-11 (Figure 1H) to further clustering, which

identified 24 transcriptionally-defined neuronal populations (Figure 2A–C). The cell groups that we identified are largely consistent with a recently published VMH_{VL}-focused single-cell (sc) RNA-seq study (Figure 2 – supplement 1) (D.-W. Kim et al. 2019). While our study identified 24 clusters whose major markers were evenly distributed between the dorsomedial and ventrolateral compartments of the VMH, Kim *et al.* identified 31 clusters with a bias toward populations with VMH_{VL} markers. Integrating the datasets (Figure 2 – supplement 1) revealed their broad correspondence, with highly correlated expression profiles (Figure 2 – supplement 1B) and shared marker genes (Figure 2 – supplement 1D). The omission of *Nfib*-marked populations from the Kim *et al.* analysis (D.-W. Kim et al. 2019) represented a notable difference between our analyses, however. In our reanalysis of their data, we found that *Nfib*-marked cells were present in their samples, but were filtered out before the final VMH clustering (Figure 2 – supplement 1). A previous scRNA-seq study of the neighboring ARC also mapped a neuron population marked by *Nfib* expression to the VMH, however (Campbell et al. 2017), and these cells correlated to our *Nfib*-marked VMH neuron populations (Figure 2 – supplement 2).

A simplified parceling scheme defines anatomically-distinct VMH neuron populations

Hierarchical clustering and marker gene analysis for our 24 mouse VMH neuron clusters using CELLEX (Timshel, Thompson, and Pers 2020) revealed that many cell groups were highly related to other VMH neuron clusters (Figure 2D, E; Supplementary File 3). Furthermore, many of these populations share marker gene expression to an

extent that renders it impossible to specifically manipulate single populations given current approaches that use a single gene for cell type manipulation (e.g., Cre-based mouse models) (Figure 2D, E). To identify classes of genetically distinguishable cells, we cut the hierarchical tree at different levels and measured the maximum pairwise expression correlation to highlight the level at which few pairs of clusters exhibited highly correlated transcriptomes. We found that 6 classes represented the largest number of classes that retained minimal correlated expression (Figure 2F). To avoid confusion, we refer to these as VMH neuron classes, while referring to the cell groups of which each class is composed as clusters or subpopulations. The mean silhouette width (a measure of clustering robustness) for the various tree cuts also supported the use of 6 classes (Figure 2 – supplement 3), and these 6 classes corresponded to the cluster designations from the broader neuron dataset (Figure 2G). Hence, a parceling scheme for mouse VMH neurons that contains 6 classes, each composed of highly similar subpopulations, captures the transcriptional patterns of the VMH. Importantly, this approach identified numerous specific marker genes (e.g., *Dlk1*, *Esr1*, *Nfib*, *Foxp2*, *Fezf1*, and *Lepr*) for each class of mouse VMH neurons (Figure 2D, H, Supplementary File 4), which should facilitate their manipulation and study.

Consistent with the distinct nature of these 6 VMH neuron classes and the utility of this parceling scheme, each class demonstrated a circumscribed anatomic distribution. As previously reported (Lee et al. 2014; Persson-Augner et al. 2014), *Dlk1*- and *Esr1*-expressing neurons (VMH^{Dlk1} and VMH^{Esr1}, respectively) map to the VMH_{VL}. While *Dlk1* is unique to a single class of VMH neurons, it is also expressed in neighboring hypothalamic neurons (Figure 2 – supplement 4), complicating its utility for

manipulating this population without using an intersectional approach. In contrast to these ventrolateral populations, *Lepr*-expressing cells lie within the core of the VMH_{DM} (Elmquist et al. 1998) and the expression of marker genes for the *Nfib*-marked clusters (VMH^{Nfib}) resides in the most dorsomedial compartment of the VMH_{DM} (Figure 2 – supplement 5). *Fezf1*-marked populations (VMH^{Fezf1}) include cells with similarity to both ventrolateral VMH^{Dlk1} and dorsomedial VMH^{Lepr} neurons, and many VMH^{Fezf1} neurons lie in VMH_C, in the transition between the dorsomedial and ventrolateral zones of the VMH. Markers for the *Foxp2*-expressing populations (VMH^{Foxp2}) reside anterior and lateral to the core of the VMH, in the so-called tuberal region (Figure 2 – supplement 6). Thus, the major VMH classes identified by our analysis each map to specific and distinct anatomic locations, consistent with their unique genetic signatures.

Lepr-directed TRAP-seq analysis of VMH^{Lepr} cells

Given that *Lepr*-expressing VMH neurons mediate only a subset of VMH_{DM} functions, we were intrigued by the finding that unbiased snRNA-seq identified a distinct class of VMH_{DM} cells marked by *Lepr* (VMH^{Lepr} neurons), consistent with a specialized role for *Lepr*-expressing VMH cells (Minokoshi, Haque, and Shimazu 1999; Toda et al. 2013; Noble et al. 2014; Gavini, Jones, and Novak 2016). The finding that *Lepr*-expressing VMH neurons map onto a single VMH neuron class also suggests a uniformity of function for these cells, which contrasts with the situation in other brain regions (such as the neighboring ARC, where multiple cell types with opposing functions (e.g., *Agrp* and *Pomc* cells) express *Lepr* (Campbell et al. 2017)). We utilized TRAP-seq to assess the extent to which *Lepr*-expressing VMH neurons correspond to the VMH^{Lepr} clusters and to compare the genetic program of *Lepr*-expressing VMH

neurons with gene expression in snRNA-seq-defined VMH neuron classes and subpopulations.

TRAP-seq analysis of microdissected VMH tissue from *Lepr*^{Cre}*;Rosa26*$^{eGFP\text{-}L10a}$ animals (Leshan et al. 2006) resulted in the enrichment of transcripts from *Lepr*^{Cre} neurons that lie in VMH-adjacent brain areas, including *Agrp*-, *Ghrh*-, *Pomc*- and *Nts*-expressing cells from the ARC and lateral hypothalamic area (LHA) (Figure 3 – supplement 1). To more closely restrict our TRAP-seq analysis to *Lepr*-expressing neurons that reside in the VMH, we used a recently developed mouse line that expresses eGFP-L10a only in cells that contain both Cre and Flp recombinases (Sabatini et al. 2021). Because VMH neurons contain vGLUT2 (encoded by *Slc17a6*), while most *Lepr*-expressing neurons in the neighboring ARC, dorsomedial hypothalamus (DMH), and LHA do not (Vong et al. 2011), we crossed a *Slc17a6*^{Flpo} mouse line to *Lepr*^{Cre} and *RCFL*$^{eGFP\text{-}L10}$ to produce *Slc17a6*^{Flpo}*; Lepr*^{Cre}; *RCFL*$^{eGFP\text{-}L10}$ (Lepr^{Slc17a6}-L10a) mice. In these mice, mediobasal hypothalamic eGFP-L10a was largely restricted to the VMH (Figure 3A) (Sabatini et al. 2021).

We microdissected the VMH of Lepr^{Slc17a6}-L10a mice and performed TRAP-seq, identifying 3,580 transcripts that were enriched in the TRAP material relative to the supernatant (Figure 3C, Supplementary File 5). Importantly, *Lepr* itself was not enriched, suggesting that we successfully purified ribosome-associated mRNA from *Lepr*-expressing VMH cells away from that derived from other *Lepr*-expressing populations (Figure 3B). We found that most non-VMH genes enriched in our conventional (*Lepr*^{Cre}-only) TRAP-Seq (including *Agrp*, *Nts*, and *Ghrh*) were not enriched in this analysis (Figure 3 – supplement 1). *Pomc* and *Prlh* remained somewhat enriched, however,

suggesting that *Lepr*-expressing DMH *Prlh* cells are glutamatergic (Dodd et al. 2014), and consistent with the finding that some ARC *Pomc* cells express *Slc17a6* (Jones et al. 2019).

As expected, we observed a high degree of concordance between snRNA-seq-defined gene expression in neurons of the VMH^{Lepr} cluster with gene expression in *Lepr*-expressing VMH neurons by TRAP-seq. We identified 3,576 genes enriched in VMH-centered $Lepr^{Slc17a6}$ TRAP-seq material (Figure 3C), 1,174 of which were also enriched in pseudo-TRAP analysis of the neurons assigned to the VMH^{Lepr} population (Supplementary File 6). Among the top enriched genes shared by these two methods were *Gpr149*, *Rai14*, and *Tnfrsf8* (Figure 3F), which exhibit a similar VMH_{DM}-centered expression pattern as *Lepr* (Figure 3G-I). As with the *Nr5a1-Cre* TRAP-seq, enrichment was largely a function of expression level: the genes that were enriched in both datasets were highly expressed in both, while the genes that were specific to TRAP or pseudo-TRAP were highly expressed in their enriched dataset, but more lowly expressed in the other. Notably, gene ontology analysis of the common genes revealed many terms related to synaptic function, while genes unique to TRAP-seq were enriched for ribosomal and mitochondrial function (data not shown).

We mapped enriched genes from $Lepr^{Slc17a6}$ TRAP-seq to the gene expression profiles of our snRNA-seq-defined VMH neuron populations (Figure 3F), revealing the bias of $Lepr^{Slc17a6}$ TRAP-seq gene expression toward VMH^{Lepr} neurons and the exclusion of markers from other VMH^{Lepr} cells from $Lepr^{Slc17a6}$ TRAP-seq-enriched genes. Thus, this analysis demonstrates that *Lepr*-expressing VMH neurons map

specifically to VMH^{Lepr} cell clusters, suggesting that they represent a transcriptionally and functionally unique set of neurons.

Conservation of VMH neuronal populations across species

While many previous studies of VMH neuron function have suggested that this brain region contains neurons that could represent therapeutic targets to aid people with obesity, diabetes, and other diseases, most of these studies have been performed in mice (Hashikawa et al. 2017; Flak et al. 2020; Meek et al. 2013; K. W. Kim et al. 2012). We know little about the cross-species conservation of VMH cell populations, however. To assess the potential conservation of VMH neuron populations across species, we microdissected macaque (*Macaca mulatta*) VMH and performed snRNA-seq using the same techniques as for mouse VMH (Figure 4 – supplement 1). A subset of macaque neurons expressed *NR5A1* and/or *FEZF1* and exhibited similar gene expression profiles to our mouse *Nr5a1-Cre* TRAP-seq enriched genes (Figure 4 – supplement 2), suggesting that these cells represent the macaque VMH and indicating that the mouse and macaque VMH share similar global gene expression signatures.

Graph-based clustering of the macaque VMH neurons yielded 7 populations with unique marker genes (with the partial exception of two related *ESR1*-expressing cell types) (Figure 4B–E). Most of these macaque populations, including populations marked by *LEPR*, *FOXP2*, *NFIB* and *ESR1* (VMH^{LEPR}, VMH^{FOXP2}, VMH^{NFIB}, and VMH^{ESR1}, respectively), have presumptive orthologs in the mouse (Figure 4D, see Supplementary File 7 for a complete list of markers). While populations marked by *DLK1* and *FEZF1* were absent from this analysis, the macaque VMH contained a population marked by *QRFPR* expression (VMH^{QRFPR}).

To determine whether the macaque populations were orthologous to those from the mouse, we first compared expression of orthologous genes among mouse and macaque cell clusters. We found that all macaque populations had clear correlates in the mouse, which mapped according to their marker genes (as expected) (Figure 4F, Figure 5 – supplement 1D). Notably, the macaque VMH^{QRFPR} population correlated with clusters from both VMH^{Dlk1} and VMH^{Fezf1} classes in the mouse, suggesting that VMH^{QRFPR} contains orthologs of the mouse VMH^{Dlk1} and VMH^{Fezf1} classes. Projecting the mouse or macaque cluster labels onto the other species using Seurat anchors (see Methods for more detail) yielded similar results (Figure 5 – supplement 1). All major classes from mouse and macaque projected with high confidence onto the equivalent major classes of the other species, and the macaque VMH^{QRFPR} population was represented by both mouse VMH^{Dlk1} and VMH^{Fezf1} cells (Figure 5 – supplement 1A).

To generate an atlas of conserved mouse and macaque VMH populations, we integrated the mouse and macaque data and clustered the merged dataset using the Seurat CCA framework (Figure 5A–B, see Methods for more detail). This analysis revealed populations of VMH neurons that each contained mouse and macaque cells in roughly equal proportions (Figure 5E). As predicted, neurons from the macaque VMH^{LEPR}, VMH^{FOXP2}, VMH^{NFIB}, and VMH^{ESR1} classes mapped directly with murine VMH^{Lepr}, VMH^{Foxp2}, VMH^{Nfib} and VMH^{Esr1} classes, respectively (Figure 5G). We examined the potential co-expression of conserved marker genes for VMH^{LEPR} cells by *in situ* hybridization (ISH) for *ACVR1C* in the macaque hypothalamus (Figure 5 – supplement 2), confirming *ACVR1C* is co-expressed with *LEPR* in the macaque VMH_{DM}. We also examined the potential co-expression of *SLC17A8* (which marks VMH^{NFIB}) with

LEPR. SLC17A8 identified a population of cells that lay at the medial extreme of the macaque VMH_{DM}, corresponding to the most dorsomedial aspect of the rodent VMH_{DM}, as for murine VMH^{Nfib} cells; these cells did not colocalize with *LEPR*-expressing cells (Figure 5 – supplement 2).

This analysis also identified macaque populations that mapped with the murine VMH^{Dlk1} and VMH^{Fezf1} populations; these derived mainly from the macaque VMH^{QRFPR} population (Figure 5G). Notably, *FEZF1* and *DLK1* were poorly enriched in the macaque VMH^{QRFPR} population (Figure 5D), while mouse *Qrfpr* expression was biased toward the VMH^{Esr1} populations (Figure 5D). Despite differences in some marker genes, however, the orthologous macaque and mouse VMH neuron populations share dozens of other genes across species (Figure 5H, Supplementary File 8, Figure 5 – supplement 1B), suggesting that the mouse and macaque cells in each group represent similar cell types. GO analysis of common marker genes (Supplementary File 9, Supplementary File 10) revealed that most of these mediate core neuronal functions, such as ion channel activity (Figure 5 – supplement 1C). Thus, while some marker genes vary across species, the mouse VMH populations have close orthologs in the macaque VMH based upon their gene expression profiles.

DISCUSSION

We combined TRAP- and snRNA-seq analysis of the VMH to identify 24 mouse neuronal populations with complex interrelations. These 24 populations represented six distinct cell classes that demonstrated unique anatomic distribution patterns. The main VMH classes were highly conserved between the mouse and the macaque in terms of gene expression profiles and anatomic distribution within the VMH. This atlas of conserved VMH neuron populations provides an unbiased and tractable starting point for the analysis of VMH circuitry and function.

Having many populations of VMH neurons with highly related gene expression profiles complicates the functional analysis of VMH cell types, suggesting the importance of simplifying the map of these heterogeneous populations to permit their manipulation and study. By using hierarchical clustering, we were able to identify six maximally unrelated classes of VMH neurons with distinct gene expression signatures. These six discrete transcriptionally-defined VMH neuronal classes demonstrated distinct anatomic distribution patterns (three located in the VMH_{DM}, two in the VMH_{VL}, and one in the tuberal region), revealing a transcriptional basis for the previously-suggested functional architecture of the VMH.

Our VMH cell populations were similar to those previously described by Kim *et al*., although they more finely split the VMH_{VL} populations than did we (presumably because their dissection bias toward the VMH_{VL} yielded more VMH_{VL} neurons) (D.-W. Kim et al. 2019). We were able to more clearly distinguish among VMH_{DM} cell types in our VMH_{DM}-focused analysis, however, including by dividing the VMH_{DM} neurons that they identified into two major classes (VMH^{Lepr} and VMH^{Fezf1}), as well as identifying a third

VMH_{DM} population (VMH^{Nfib}) absent from their analysis. Interestingly, the VMH^{Nfib} population was quite distinct from the more closely related VMH^{Lepr} and VMH^{Fezf1} VMH_{DM} cell types, suggesting a potentially divergent function for this most dorsomedial of the VMH_{DM} populations.

Our mouse VMH cell types mapped clearly onto specific populations of macaque VMH neurons, revealing the utility of the mouse as a surrogate for the primate in terms of VMH cell types and, presumably, function. While the macaque single VMH^{QRFRP} population mapped to two mouse classes (VMH^{Fezf1} and VMH^{Dlk1}) by orthologous gene expression, these mouse classes are closely related to each other (transcriptionally and anatomically) and the macaque cells from VMH^{QRFRP} segregate to distinct cell clusters defined by *Dlk1* and *Fezf1* in the mouse when we integrated and reclustered the mouse and macaque cell data. Also, while *DLK1* is not specific to the macaque VMH^{QRFPR} cells, the otherwise similar gene expression profiles of mouse and macaque cells that map to VMH^{Dlk1} or VMH^{Fezf1} populations suggests the conserved nature of these cell types across species.

While not all *Lepr*-expressing cell types track in the brain across species (e.g., preproglucagon (*Gcg*)-containing NTS neurons in the mouse express *Lepr*, rat NTS *Gcg* cells do not (Huo et al. 2008)), mouse VMH^{Lepr} neurons map directly with macaque VMH^{LEPR} neurons by all of the measures that we examined. The finding that *Lepr/LEPR* expression marks a unique and conserved cell type in rodent and primate is consistent with the notion that this class of VMH neuron mediates a discrete component of VMH function, as suggested by previous work in the mouse demonstrating roles for *Lepr*-

358 expressing VMH neurons in the control of energy balance, but not glucose production or
359 panic-like behaviors (Meek et al. 2013; 2016; Sabatini et al. 2021).

360 While the tuberal region contains more GABAergic than glutamatergic neurons,
361 this region projects to similar target areas as does the core VMH and contains
362 substantial numbers of neurons marked by *Nr5a1-Cre* activity. Hence, although
363 VMH^{Foxp2} cells lie in the tuberal region, their glutamatergic nature, their marking by
364 *Nr5a1-Cre* activity, and the finding that they are transcriptional most similar to other
365 VMH populations mark VMH^{Foxp2} cells as VMH neurons. While few data exist to suggest
366 the physiologic roles played by these cells, it will be interesting to manipulate VMH^{Foxp2}
367 neurons to determine their function.

368 The identification of distinct transcriptionally-defined VMH cell populations
369 provides the opportunity to develop new tools that can be used to understand the nature
370 and function of VMH_{DM} cell types and their roles in metabolic control. The finding that
371 the major VMH cell classes found in the mouse are present in the macaque support the
372 use of the mouse to study the metabolic functions of the VMH as a means to identify
373 potential therapeutic targets for human disease. It will be important to use these
374 findings to dissect functions for subtypes of VMH cells, which may represent targets for
375 the therapy of diseases including obesity and diabetes.

Methods

Animals

Mice were bred in the Unit for Laboratory Animal Medicine at the University of Michigan. These mice and the procedures performed were approved by the University of Michigan Committee on the Use and Care of Animals and in accordance with Association for the Assessment and Approval of Laboratory Animal Care (AAALAC) and National Institutes of Health (NIH) guidelines. Mice were provided with *ad libitum* access to food (Purina Lab Diet 5001) and water in temperature-controlled (25°C) rooms on a 12 h light-dark cycle with daily health status checks.

Nr5a1-Cre (Jax: 012462) (Dhillon et al. 2006) and *Foxp2*$^{IRES\text{-}Cre}$ (Jax: 030541) (Rousso et al. 2016) mice were obtained from Jackson Laboratories. *Rosa26*$^{CAG\text{-}LSL\text{-}eGFP\text{-}L10a}$, *Lepr*^{Cre} (Jax: 032457), *Slc17a6*^{Flpo} and *RCFL*$^{eGFP\text{-}L10a}$ mice have been described previously(Leshan et al. 2006; Krashes et al. 2014; Sabatini et al. 2021).

Nonhuman primate tissue was obtained from the Tissue Distribution Program at ONPRC. Animal care is in accordance with the recommendations described in the Guide for the Care and Use of Laboratory Animals of the NIH and animal facilities at the Oregon National Primate Research Center (ONPRC) are accredited by AAALAC.

Tissue prep, cDNA amplification and library construction for 10x snRNA-seq

Mice were euthanized using isoflurane and decapitated, the brain was subsequently removed from the skull and sectioned into 1mm thick coronal slices using a brain matrix. The VMH was dissected out and flash frozen in liquid N_2. Nuclei were isolated as previously described (Habib et al. 2017) with modifications as follows. On

399 the day of the experiment, frozen VMH (from 2 – 3 mice) was homogenized in Lysis
400 Buffer (EZ Prep Nuclei Kit, Sigma) with Protector RNAase Inhibitor (Sigma) and filtered
401 through a 30μm MACS strainer (Myltenti). Strained samples were centrifuged at 500 rcf
402 x 5 minutes and pelleted nuclei were resuspended in washed with wash buffer (10mM
403 Tris Buffer pH 8.0, 5mM KCl, 12.5mM $MgCl_2$, 1% BSA with RNAse inhibitor). Nuclei
404 were strained again and recentrifuged at 500rcf x 5 minutes. Washed nuclei were
405 resuspended in wash buffer with propidium iodide (Sigma) and stained nuclei
406 underwent FACS sorting on a MoFlo Astrios Cell Sorter. Sorted nuclei were centrifuged
407 at 100rcf x 6 minutes and resuspended in wash buffer to obtain a concentration of 750 –
408 1200 nuclei/uL. RT mix was added to target ~10,000 nuclei recovered and loaded onto
409 the 10x Chromium Controller chip. The Chromium Single Cell 3' Library and Gel Bead
410 Kit v3, Chromium Chip B Single Cell kit and Chromium i7 Multiplex Kit were used for
411 subsequent RT, cDNA amplification and library preparation as instructed by the
412 manufacturer. Libraries were sequenced on an Illumina HiSeq 4000 or NovaSeq 6000
413 (pair-ended with read lengths of 150 nt) to a depth of at least 50,000 reads/cell.
414
415 snRNA-seq data analysis
416 Count tables were generated from the FASTQ files using cellranger and
417 analyzed in R 3.6.3 using the Seurat 3 framework. Genes expressed in at least 4 cells
418 in each sample and were not gene models (starting with "Gm") or located on the
419 mitochondrial genome were retained. Cells with at least 500 detected genes were
420 retained. Doublets were detected using Scrublet (Wolock, Lopez, and Klein 2019). For
421 each 10x run, the expected number of doublets was predicted using a linear model

given 10x data of the detected doublet rate and the number of cells. Then, each cell was given a doublet score with Scrublet and the n cells (corresponding to the expected number of doublets) with the top scores were removed.

The data was then normalized using scran (Lun, McCarthy, and Marioni 2016) and centered and scaled for each dataset independently and genes that were called variable by both Seurat *FindVariableFeatures* and sctransform (Hafemeister and Satija 2019) were input to PCA. The top PCs were retained at the “elbow” of the scree plot (normally 15-30, depending on the dataset) and then used for dimension reduction using UMAP and clustering using the Seurat *FindNeighbors* and *FindClusters* functions. Both were optimized for maximizing cluster consistency by clustering over a variety of conditions: first, varying the number of neighbors from 10 to the square root of the number of cells while holding the resolution parameter in *FindClusters* at 1 and finding the clustering that maximized the mean silhouette score; then, this number of neighbors was held fixed while varying the resolution parameter in *FindClusters* from 0.2 upward in steps of 0.2 until a maximal mean silhouette score was found. Clusters were then hierarchically ordered based on their Euclidean distance in PC space and ordered based on their position in the tree.

Marker genes were found using the Seurat function *FindAllMarkers* for each sample with resulting p-values combined using the *logitp* function from the metap package or using CELLEX 1.0.0. Cluster names were chosen based on genes found in this unbiased marker gene search and known marker genes.

From the all-cell data, cell types were predicted using gene set enrichment analysis from the marker genes and a manually curated set of genes known to mark

specific CNS cell types. From this, clusters that were highly enriched for markers from 2 (or more) distinct cell types were labeled as “doublets” and those with no enrichment were labeled as “junk”, the remaining clusters were labeled based on their lone CNS cell type.

To predict VMH neurons from all neurons, we first found genes significantly enriched in the bead fraction in *Nr5a1-Cre* TRAP-seq (see below for details) and expressed above 1 count per million. The scaled count matrix containing these genes was then used as input to PCA. The magnitude of the first principal component (loading) was then used to generate a VMH similarity score and the clusters that had a high *Nr5a1-Cre* TRAP loading, were glutamatergic (express *Slc17a6* and not *Gad1* or *Slc32a1* above the mean value), and expressed either *Nr5a1* or *Fezf1* above the mean value were included as presumptive VMH.

TRAP-seq analysis

Mice (*Lepr*^{Cre};*ROSA26*$^{EGFP\text{-}L10a}$ or *Lepr*^{Cre};*Slc17a6*^{FlpO};*ROSA26*$^{EGFP\text{-}L10a}$) were euthanized and decapitated, the brain was subsequently removed from the skull and sectioned into 1mm thick coronal slices using a brain matrix. The VMH or hypothalamus was dissected and homogenized in lysis buffer. Between 15-20 mice were used for TRAP experiments. GFP-tagged ribosomes were immunoprecipitated and RNA isolated as previously described (Allison et al. 2018). RNA was subject to ribodepletion and the resultant mRNA was fragmented and copied into first strand cDNA. The products were purified and enriched by PCR to create the final cDNA library. Samples were sequenced

on a 50-cycle single end run on a HiSeq 2500 (Illumina) according to manufacturer's protocols.

FASTQ files were filtered using fastq_quality_filter from fastx_toolkit to remove reads with a phred score < 20. Then reads were mapped using STAR with a custom genome containing the Ensembl reference and sequences and annotation for *Cre* and *EGFP:L10a* (and *Flpo* in the RCFL::eGFP-L10a dataset). Count tables were generated using the STAR --quantMode GeneCounts flag.

Count tables were analyzed in R 3.6.3 and were subject to quality control to ensure read adequate library size (20-30 million reads), enrichment of positive control genes (e.g. *EGFP:L10a* and/or *Cre, Nr5a1*), and appropriate sample similarity in both hierarchical clustering of Euclidean distance and TSNE/UMAP space (e.g. bead samples are more similar to one another than to any sup sample). All samples passed quality control. Enriched genes were determined using DESeq2 including an effect of sample pair in the model to account for pairing of the bead–sup samples (~ pair + cells).

Integration with published data

Count tables from Kim et al. (D.-W. Kim et al. 2019) were downloaded from https://data.mendeley.com/datasets/ypx3sw2f7c/3 and count tables from Campbell et al. (Campbell et al. 2017) were downloaded from https://www.ncbi.nlm.nih.gov/geo/query/acc.cgi?acc=GSE93374. Note: only the 10x data from Kim et al. was used. The data was then preprocessed and clustered in the same way as above, though some samples were removed from the Kim et al. dataset for low mean read depth that confounded clustering (Samples 2018_0802, 2018_0803,

2018_0812_1, 2018_0812_2, and 2018_0812_3). For the Kim et al. dataset, cells were clustered as above (*FindNeighbors* then *FindClusters*), and neuron clusters were predicted using WGCNA to identify correlated gene expression modules. The modules contained dozens of genes that mapped clearly onto a small set of clusters in UMAP space and—based on known marker genes—corresponded to the most prevalent cell types in the brain (e.g. neurons, astrocytes, microglia, oligodendrocytes, etc.). For the Campbell et al. data, neurons were labeled in the metadata from the authors, so neuronal barcodes were simply selected based on their annotation. For both neuronal datasets, VMH neurons were predicted using the same procedure as above: clusters that were glutamatergic, *Fezf1*/*Nr5a1*-expressing, and similar to *Nr5a1-Cre* TRAP-seq. This corroborated the clusters called VMH in both datasets by the original authors, with the exception of the *Nfib* populations in the Kim et al. dataset that was not called VMH and therefore not assigned a cluster name; we refer to these cells as (Missing) in our integrated dataset.

To find shared populations across datasets we took 2 approaches. First, variable genes were found for both datasets using the Seurat *FindVariableFeatures* function. Then, the pair-wise Pearson correlation was found for the mean scaled expression in each cluster in each dataset for the set of genes called variable in both datasets. Additionally, we used the Seurat *FindTransferAnchors* and *IntegrateData* functions to generate a merged dataset that was then subjected to PCA, UMAP reduction, and clustering in the same way as above. These new clusters containing cells from both datasets were then manually named using marker genes from the original datasets (e.g. *Dlk1*, *Esr1*, *Satb2*, *Lepr*, *Nfib*, *Foxp2*, etc.).

513

514 Immunostaining

515 Animals were perfused with phosphate buffered saline for five minutes followed
516 by an additional five minutes of 10% formalin. Brains were then removed and post-fixed
517 in 10% formalin for 24 hours at room temperature, before being moved to 30% sucrose
518 for 24 hours for a minimum of 24 hours at room temperature. Brains were then
519 sectioned as 30 μm thick free-floating sections and stained. Sections were treated with
520 blocking solution (PBS with 0.1% triton, 3% normal donkey serum; Fisher Scientific) for
521 at least 1 hour. The sections were incubated overnight at room temperature in was
522 preformed using standard procedures. The following day, sections were washed and
523 incubated with fluorescent secondary antibodies with species-specific Alexa Fluor-488
524 or -568 (Invitrogen, 1:250) to visualize proteins. Primary antibodies used include: GFP
525 (1:1000, #1020, Aves Laboratories) and NFIA (1:500, #PA5-35936, Invitrogen). Images
526 were collected on an Olympus BX51 microscope. Images were background subtracted
527 and enhanced by shrinking the range of brightness and contrast in ImageJ.

528

529 Macaque snRNA-seq

530 Whole Rhesus macaque brains were obtained from the Tissue Distribution
531 Program at ONPRC. Brains were centered within a chilled brain matrix (ASI Instruments,
532 catalog # MBM-2000C) and 2mm slices were obtained from rostral to caudal. Slices
533 containing the hypothalamus were placed in saline and the PVH, ARC, VMH and DMH
534 were punched out and samples were placed in pre-chilled tubes on dry-ice. Samples

were stored at -80C until shipment on dry ice. Nuclei were isolated from frozen macaque tissue as described above for mice.

The FASTQ files were mapped to the macaque genome (Mmul_10) using cellranger and count matrix files were analyzed in R using Seurat 3 as above, with the exception that gene models and genes mapping to the macaque mitochondrial genome were not removed. Macaque neurons were predicted using orthologs of mouse cell type marker genes and macaque VMH neurons were identified using macaque orthologs of *Nr5a1-Cre* TRAP-seq enriched genes. Orthologs were identified using Ensembl and only 1:1 orthologs were retained.

Species integration

The mouse and macaque datasets were integrated in a similar way to integrating the Kim et al. and Campbell et al. mouse datasets. First, the macaque genes were renamed to their mouse orthologs and only 1:1 orthologs and genes expressed in both species were retained. Importantly, because our dataset was biased toward the dorsomedial VMH and the Kim et al. dataset was biased toward the ventrolateral VMH, we also included 4 randomly chosen samples from the Kim et al. data to get a more representative picture of shared VMH populations across species. The data was then preprocessed, normalized, and scaled in the same way as previously. The mouse and macaque data was then integrated using the Seurat *FindTransferAnchors* and *IntegrateData* functions and marker genes were found that were common across species by running *FindAllMarkers* for each species separately and then using the metap *logitp* function to find genes that are significantly enriched.

Macaque in situ hybridization

Whole Rhesus macaque brains were obtained from the Tissue Distribution Program at ONPRC. Hypothalamic blocks fixed with 4% paraformaldehyde were incubated in glycerol prior to freezing with isopentane. Tissue was sectioned at 25 μm using a freezing stage sliding microtome and free-floating sections were stored in glycerol cryoprotectant at -20 °C. Tissue was mounted on slides prior to in situ hybridization, which was performed using ACD Bio RNAScope reagents (Multiplex Fluorescent Detection Kit v2, 323100) for Acvr1c (ACD 591481), Slc17a8 (ACD 543821-c2) and Lepr (ACD 406371-C3). Negative and positive control probes were included in all runs. Slides were imaged on an Olympus VS110 Slidescanner and processed using Visiopharm software.

Statistical Analysis

All data is displayed as mean +/- SEM. All plotting and statistical analysis was performed using R 3.6.3. Specific statistical tests are listed in the figure legends.

Resource availability

All mouse strains will be made available upon reasonable request.

Data availability

Sequencing data, count matrices, and metadata for all experiments are available through GEO at accession number GSE172207.

Code availability

All analysis code will be available at github.com/alanrupp/affinati-2021.

Acknowledgments: We thank Randy Seeley, Lotte Bjerre Knudsen, Kevin Grove, Mads Tang-Christensen, Christine Bjørn Jensen and members of the Myers and Olson labs for helpful discussions. Research support was provided by the Michigan Diabetes Research Center (NIH P30 DK020572, including the Molecular Genetics, Microscopy, and Animal Studies Cores), the Marilyn H. Vincent Foundation (to MGM), Novo Nordisk A/S (to MGM), ADA 1-19-PDF-099 (to PVS) and NIH DK122660 (to AHA). NHP data was supported by National Institutes of Health Grant P51 OD-11092 for operation of the Oregon National Primate Research Center and DK123115 (PK).

References

Allison, Margaret B., Warren Pan, Alexander MacKenzie, Christa Patterson, Kimi Shah, Tammy Barnes, Wenwen Cheng, Alan Rupp, David P. Olson, and Martin G. Myers. 2018. “Defining the Transcriptional Targets of Leptin Reveals a Role for *Atf3* in Leptin Action.” *Diabetes* 67 (6): 1093–1104. https://doi.org/10.2337/db17-1395.

Bingham, Nathan C., Sunita Verma-Kurvari, Luis F. Parada, and Keith L. Parker. 2006. “Development of a Steroidogenic Factor 1/Cre Transgenic Mouse Line.” *Genesis* 44 (9): 419–24. https://doi.org/10.1002/dvg.20231.

Campbell, John N., Evan Z. Macosko, Henning Fenselau, Tune H. Pers, Anna Lyubetskaya, Danielle Tenen, Melissa Goldman, et al. 2017. “A Molecular Census of Arcuate Hypothalamus and Median Eminence Cell Types.” *Nature Neuroscience* 20 (3): 484–96. https://doi.org/10.1038/nn.4495.

Chen, Hong, Olga Charlat, Louis A Tartaglia, Elizabeth A Woolf, Xun Weng, Stephen J Ellis, Nathan D Lakey, et al. 1996. “Evidence That the Diabetes Gene Encodes the Leptin Receptor: Identification of a Mutation in the Leptin Receptor Gene in Db/Db Mice.” *Cell* 84 (3): 491–95. https://doi.org/10.1016/S0092-8674(00)81294-5.

Chen, Renchao, Xiaoji Wu, Lan Jiang, and Yi Zhang. 2017. “Single-Cell RNA-Seq Reveals Hypothalamic Cell Diversity.” *Cell Reports* 18 (13): 3227–41. https://doi.org/10.1016/j.celrep.2017.03.004.

Cheung, Clement C., Deborah M. Kurrasch, Jenna K. Liang, and Holly A. Ingraham. 2013. “Genetic Labeling of Steroidogenic Factor-1 (SF-1) Neurons in Mice Reveals Ventromedial Nucleus of the Hypothalamus (VMH) Circuitry Beginning at Neurogenesis and Development of a Separate Non-SF-1 Neuronal Cluster in the Ventrolateral VMH.” *Journal of Comparative Neurology* 521 (6): 1268–88. https://doi.org/10.1002/cne.23226.

Dhillon, Harveen, Jeffrey M. Zigman, Chianping Ye, Charlotte E. Lee, Robert A. McGovern, Vinsee Tang, Christopher D. Kenny, et al. 2006. “Leptin Directly Activates SF1 Neurons in the VMH, and This Action by Leptin Is Required for Normal Body-Weight Homeostasis.” *Neuron* 49 (2): 191–203. https://doi.org/10.1016/j.neuron.2005.12.021.

Dodd, Garron T., Amy A. Worth, Nicolas Nunn, Aaron K. Korpal, David A. Bechtold, Margaret B. Allison, Martin G. Myers, Michael A. Statnick, and Simon M. Luckman. 2014. “The Thermogenic Effect of Leptin Is Dependent on a Distinct Population of Prolactin-Releasing Peptide Neurons in the Dorsomedial Hypothalamus.” *Cell Metabolism* 20 (4): 639–49. https://doi.org/10.1016/j.cmet.2014.07.022.

Elmquist, J. K., C. Bjørbaek, R. S. Ahima, J. S. Flier, and C. B. Saper. 1998. “Distributions of Leptin Receptor MRNA Isoforms in the Rat Brain.” *The Journal of Comparative Neurology* 395 (4): 535–47.

Flak, Jonathan N., Paulette B. Goforth, James Dell’Orco, Paul V. Sabatini, Chien Li, Nadejda Bozadjieva, Matthew Sorensen, et al. 2020. “Ventromedial Hypothalamic Nucleus Neuronal Subset Regulates Blood Glucose Independently of Insulin.” *Journal of Clinical Investigation* 130 (6): 2943–52. https://doi.org/10.1172/JCI134135.

Gavini, Chaitanya K., William C. Jones, and Colleen M. Novak. 2016. “Ventromedial Hypothalamic Melanocortin Receptor Activation: Regulation of Activity Energy Expenditure and Skeletal Muscle Thermogenesis: VMH and Skeletal Muscle Thermogenesis.” *The Journal of Physiology* 594 (18): 5285–5301. https://doi.org/10.1113/JP272352.

Habib, Naomi, Inbal Avraham-Davidi, Anindita Basu, Tyler Burks, Karthik Shekhar, Matan Hofree, Sourav R Choudhury, et al. 2017. “Massively Parallel Single-Nucleus RNA-Seq with DroNc-Seq.” *Nature Methods* 14 (10): 955–58. https://doi.org/10.1038/nmeth.4407.

Hafemeister, Christoph, and Rahul Satija. 2019. “Normalization and Variance Stabilization of Single-Cell RNA-Seq Data Using Regularized Negative Binomial Regression.” *Genome Biology* 20 (1): 296. https://doi.org/10.1186/s13059-019-1874-1.

Hashikawa, Koichi, Yoshiko Hashikawa, Robin Tremblay, Jiaxing Zhang, James E Feng, Alexander Sabol, Walter T Piper, Hyosang Lee, Bernardo Rudy, and Dayu Lin. 2017. “Esr1+ Cells in the Ventromedial Hypothalamus Control Female Aggression.” *Nature Neuroscience* 20 (11): 1580–90. https://doi.org/10.1038/nn.4644.

Huo, Lihong, Kevin M. Gamber, Harvey J. Grill, and Christian Bjørbaek. 2008. “Divergent Leptin Signaling in Proglucagon Neurons of the Nucleus of the

659 Solitary Tract in Mice and Rats." *Endocrinology* 149 (2): 492–97.
660 https://doi.org/10.1210/en.2007-0633.
661 Jones, Graham L., Gábor Wittmann, Eva B. Yokosawa, Hui Yu, Aaron J. Mercer,
662 Ronald M. Lechan, and Malcolm J. Low. 2019. "Selective Restoration of *Pomc*
663 Expression in Glutamatergic POMC Neurons: Evidence for a Dynamic
664 Hypothalamic Neurotransmitter Network." *Eneuro* 6 (2): ENEURO.0400-18.2019.
665 https://doi.org/10.1523/ENEURO.0400-18.2019.
666 Kim, Dong-Wook, Zizhen Yao, Lucas T. Graybuck, Tae Kyung Kim, Thuc Nghi Nguyen,
667 Kimberly A. Smith, Olivia Fong, et al. 2019. "Multimodal Analysis of Cell Types in
668 a Hypothalamic Node Controlling Social Behavior." *Cell* 179 (3): 713-728.e17.
669 https://doi.org/10.1016/j.cell.2019.09.020.
670 Kim, Ki Woo, Jose Donato, Eric D. Berglund, Yun-Hee Choi, Daisuke Kohno, Carol F.
671 Elias, Ronald A. Depinho, and Joel K. Elmquist. 2012. "FOXO1 in the
672 Ventromedial Hypothalamus Regulates Energy Balance." *The Journal of Clinical*
673 *Investigation* 122 (7): 2578–89. https://doi.org/10.1172/JCI62848.
674 Krashes, Michael J., Bhavik P. Shah, Joseph C. Madara, David P. Olson, David E.
675 Strochlic, Alastair S. Garfield, Linh Vong, et al. 2014. "An Excitatory
676 Paraventricular Nucleus to AgRP Neuron Circuit That Drives Hunger." *Nature*
677 507 (7491): 238–42. https://doi.org/10.1038/nature12956.
678 Krause, William C., and Holly A. Ingraham. 2017. "Origins and Functions of the
679 Ventrolateral VMH: A Complex Neuronal Cluster Orchestrating Sex Differences
680 in Metabolism and Behavior." In *Sex and Gender Factors Affecting Metabolic*
681 *Homeostasis, Diabetes and Obesity*, edited by Franck Mauvais-Jarvis,
682 1043:199–213. Advances in Experimental Medicine and Biology. Cham: Springer
683 International Publishing. https://doi.org/10.1007/978-3-319-70178-3_10.
684 Kunwar, Prabhat S., Moriel Zelikowsky, Ryan Remedios, Haijiang Cai, Melis Yilmaz,
685 Markus Meister, and David J. Anderson. 2015. "Ventromedial Hypothalamic
686 Neurons Control a Defensive Emotion State." *ELife* 4 (March).
687 https://doi.org/10.7554/eLife.06633.
688 Kurrasch, D. M., C. C. Cheung, F. Y. Lee, P. V. Tran, K. Hata, and H. A. Ingraham.
689 2007. "The Neonatal Ventromedial Hypothalamus Transcriptome Reveals Novel
690 Markers with Spatially Distinct Patterning." *Journal of Neuroscience* 27 (50):
691 13624–34. https://doi.org/10.1523/JNEUROSCI.2858-07.2007.
692 Lam, Brian Y.H., Irene Cimino, Joseph Polex-Wolf, Sara Nicole Kohnke, Debra
693 Rimmington, Valentine Iyemere, Nicholas Heeley, et al. 2017. "Heterogeneity of
694 Hypothalamic Pro-Opiomelanocortin-Expressing Neurons Revealed by Single-
695 Cell RNA Sequencing." *Molecular Metabolism* 6 (5): 383–92.
696 https://doi.org/10.1016/j.molmet.2017.02.007.
697 Lee, Hyosang, Dong-Wook Kim, Ryan Remedios, Todd E. Anthony, Angela Chang,
698 Linda Madisen, Hongkui Zeng, and David J. Anderson. 2014. "Scalable Control
699 of Mounting and Attack by Esr1+ Neurons in the Ventromedial Hypothalamus."
700 *Nature* 509 (7502): 627–32. https://doi.org/10.1038/nature13169.
701 Leshan, Rebecca L., Marie Björnholm, Heike Münzberg, and Martin G. Myers. 2006.
702 "Leptin Receptor Signaling and Action in the Central Nervous System." *Obesity*
703 14 (August): 208S-212S. https://doi.org/10.1038/oby.2006.310.

Lindberg, Daniel, Peilin Chen, and Chien Li. 2013. “Conditional Viral Tracing Reveals That Steroidogenic Factor 1-Positive Neurons of the Dorsomedial Subdivision of the Ventromedial Hypothalamus Project to Autonomic Centers of the Hypothalamus and Hindbrain.” *The Journal of Comparative Neurology* 521 (14): 3167–90. https://doi.org/10.1002/cne.23338.

Lun, Aaron T.L., Davis J. McCarthy, and John C. Marioni. 2016. “A Step-by-Step Workflow for Low-Level Analysis of Single-Cell RNA-Seq Data with Bioconductor.” *F1000Research* 5 (October): 2122. https://doi.org/10.12688/f1000research.9501.2.

Meek, Thomas H., Miles E. Matsen, Mauricio D. Dorfman, Stephan J. Guyenet, Vincent Damian, Hong T. Nguyen, Gerald J. Taborsky, and Gregory J. Morton. 2013. “Leptin Action in the Ventromedial Hypothalamic Nucleus Is Sufficient, but Not Necessary, to Normalize Diabetic Hyperglycemia.” *Endocrinology* 154 (9): 3067–76. https://doi.org/10.1210/en.2013-1328.

Meek, Thomas H., Jarrell T. Nelson, Miles E. Matsen, Mauricio D. Dorfman, Stephan J. Guyenet, Vincent Damian, Margaret B. Allison, et al. 2016. “Functional Identification of a Neurocircuit Regulating Blood Glucose.” *Proceedings of the National Academy of Sciences of the United States of America* 113 (14): E2073-2082. https://doi.org/10.1073/pnas.1521160113.

Minokoshi, Y., M. S. Haque, and T. Shimazu. 1999. “Microinjection of Leptin into the Ventromedial Hypothalamus Increases Glucose Uptake in Peripheral Tissues in Rats.” *Diabetes* 48 (2): 287–91. https://doi.org/10.2337/diabetes.48.2.287.

Noble, Emily E., Charles J. Billington, Catherine M. Kotz, and ChuanFeng Wang. 2014. “Oxytocin in the Ventromedial Hypothalamic Nucleus Reduces Feeding and Acutely Increases Energy Expenditure.” *American Journal of Physiology-Regulatory, Integrative and Comparative Physiology* 307 (6): R737–45. https://doi.org/10.1152/ajpregu.00118.2014.

Persson-Augner, David, Yong-Woo Lee, Sulay Tovar, Carlos Dieguez, and Björn Meister. 2014. “Delta-Like 1 Homologue (DLK1) Protein in Neurons of the Arcuate Nucleus That Control Weight Homeostasis and Effect of Fasting on Hypothalamic DLK1 MRNA.” *Neuroendocrinology* 100 (2–3): 209–20. https://doi.org/10.1159/000369069.

Rousso, David L., Mu Qiao, Ruth D. Kagan, Masahito Yamagata, Richard D. Palmiter, and Joshua R. Sanes. 2016. “Two Pairs of ON and OFF Retinal Ganglion Cells Are Defined by Intersectional Patterns of Transcription Factor Expression.” *Cell Reports* 15 (9): 1930–44. https://doi.org/10.1016/j.celrep.2016.04.069.

Sabatini, Paul V, Jine Wang, Alan C Rupp, Alison H Affinati, Jonathan N Flak, Chien Li, David P Olson, and Martin G Myers. 2021. “TTARGIT AAVs Mediate the Sensitive and Flexible Manipulation of Intersectional Neuronal Populations in Mice.” *ELife* 10 (March): e66835. https://doi.org/10.7554/eLife.66835.

Tartaglia, Louis A., Marlene Dembski, Xun Weng, Nanhua Deng, Janice Culpepper, Rene Devos, Grayson J. Richards, et al. 1995. “Identification and Expression Cloning of a Leptin Receptor, OB-R.” *Cell* 83 (7): 1263–71. https://doi.org/10.1016/0092-8674(95)90151-5.

Timshel, Pascal N, Jonatan J Thompson, and Tune H Pers. 2020. “Genetic Mapping of Etiologic Brain Cell Types for Obesity.” *ELife* 9 (September): e55851. https://doi.org/10.7554/eLife.55851.
Toda, C., T. Shiuchi, H. Kageyama, S. Okamoto, E. A. Coutinho, T. Sato, Y. Okamatsu-Ogura, et al. 2013. “Extracellular Signal-Regulated Kinase in the Ventromedial Hypothalamus Mediates Leptin-Induced Glucose Uptake in Red-Type Skeletal Muscle.” *Diabetes* 62 (7): 2295–2307. https://doi.org/10.2337/db12-1629.
Vander Tuig, Jerry G., Allen W. Knehans, and Dale R. Romsos. 1982. “Reduced Sympathetic Nervous System Activity in Rats with Ventromedial Hypothalamic Lesions.” *Life Sciences* 30 (11): 913–20. https://doi.org/10.1016/0024-3205(82)90619-1.
Vong, Linh, Chianping Ye, Zongfang Yang, Brian Choi, Streamson Chua, and Bradford B. Lowell. 2011. “Leptin Action on GABAergic Neurons Prevents Obesity and Reduces Inhibitory Tone to POMC Neurons.” *Neuron* 71 (1): 142–54. https://doi.org/10.1016/j.neuron.2011.05.028.
Wolock, Samuel L., Romain Lopez, and Allon M. Klein. 2019. “Scrublet: Computational Identification of Cell Doublets in Single-Cell Transcriptomic Data.” *Cell Systems* 8 (4): 281-291.e9. https://doi.org/10.1016/j.cels.2018.11.005.

Figure legends

Figure 1: Identification of VMH neurons from mice. (**A**) Schematic of VMH nuclei isolation and single-cell sequencing protocol. (**B**) UMAP projection of 21,585 neuronal nuclei colored and labeled by cluster designation. (**C**) Expression profile of the top enriched genes for each cluster (colored on bottom), including GABAergic (*Gad1*) and glutamatergic (*Slc17a6*) markers. (**D**) Expression of *Nr5a1* and *Fezf1* in individual cells in UMAP space. (**E**) *Nr5a1-Cre* TRAP-seq overview. *Nr5a1-Cre* mice were crossed with *ROSA26*$^{eGFP\text{-}L10a}$ mice, resulting in VMH-restricted eGFP-L10a expression. Representative image shows GFP-IR (black) in a coronal section from these mice. (**F**) TRAP-seq revealed the enrichment of thousands of genes (including *Nr5a1* and *Fezf1)* in these cells relative to non-TRAP material. (**G**) Expression profile of the top enriched genes from *Nr5a1-Cre* TRAP-seq across clusters; gray box indicates presumptive VMH cells. (**H**) Magnitude of the first principal component after performing principal components analysis for the genes enriched in *Nr5a1-Cre* TRAP-seq. (**I**) Venn diagram of genes enriched in *Nr5a1-Cre* TRAP-seq (TRAP enriched), in snRNA-seq VMH pseudo-TRAP (pseudo-TRAP enriched), or both (Common). Number in parentheses refers to the number of genes in each category. (**J**) Histograms of expression level for genes by enrichment geneset in each dataset (*Nr5a1-Cre* TRAP-seq or snRNA-seq). (**K**)

Mean scaled expression for each cluster for the top genes enriched in *Nr5a1-Cre* TRAP-seq.

Figure 2: VMH neuronal populations can be grouped into 6 major classes. (**A**) UMAP projection of 6,049 VMH neurons colored and labeled by cluster designation. (**B**) Prevalence of clusters across samples, mean ± SEM. (**C**) Expression profile of the top enriched genes for each cluster. (**D**) Hierarchical clustering and mean expression of marker genes for each class of neurons. (**E**) ESμ for the top 3 marker genes for each population determined by CELLEX. (**F**) Median maximal pairwise expression correlation for each cut of the hierarchical tree resulting in 2–24 clusters. (**G**) Percent of cells in each VMH cluster that correspond to each neuronal cluster (from Figure 1). (**H**) ESμ for the top 5 marker genes for each major class determined by CELLEX.

Figure 3: VMH^{Lepr} neurons represent a distinct class of VMH neurons. (**A**) Diagram of strategy to transcriptionally profile the VMH^{Lepr} neurons by crossing *Lepr*^{Cre} and *Slc17a6*^{Flpo} to a mouse line in which the *ROSA26* (*R26*) locus contains a CAG-driven, Flp- and Cre-dependent *eGFP:L10a* allele (*RCFL*$^{eGFP\text{-}L10a}$). (below) A representative image of GFP-IR (black) expression in *Lepr*^{Cre};*Slc17a6*^{Flpo};*RCFL*$^{eGFP\text{-}L10a}$ ($Lepr^{Slc17a6}$-L10a) mice. (**B**) Scaled counts per million (CPM) for each gene in $Lepr^{Slc17a6}$-L10a mice. (**C**) Expression and enrichment of genes from $Lepr^{Slc17a6}$-L10a VMH pulldown. (**D**) Expression of *Lepr* in individual VMH neurons in UMAP space. (**E**) Magnitude of the first principal component after performing principal components analysis for the genes enriched in $Lepr^{Slc17a6}$-L10a VMH TRAP-seq, projected into UMAP space. (**F**) Mean class expression (left), Lepr cluster expression (center), and $Lepr^{Slc17a6}$-L10a TRAP-seq enrichment (right) of the top genes unique to the VMH^{Lepr} population by both TRAP and pseudo-TRAP. (**G**–**I**) Sagittal Allen Brain Atlas *in situ* images for (**G**) *Gpr149*, (**H**) *Rai14*, and (**I**) *Tnfrsf8*; all probes shown in black.

Figure 4: Macaque VMH populations revealed by snRNA-seq. (**A**) Schematic of experimental process for macaque snRNA-seq. (**B**) UMAP projection of 3,752 VMH neuronal nuclei colored and labeled by cluster designation. (**C**) Expression profile of the

top enriched genes for each cluster. (**D**) Violin plot of normalized expression for marker genes for each VMH neuronal population. (**E**) ESμ for the top 5 marker genes for each cluster determined by CELLEX. (**F**) Pairwise scaled expression correlation (Pearson's r) for each macaque and mouse VMH neuronal cluster.

Figure 5: VMH populations are conserved between mouse and macaque. (**A**–**B**) Mouse and macaque snRNA-seq datasets were (**A**) merged using canonical correlation analysis and (**B**) projected onto UMAP space, colored here by species. (**C**) UMAP projection of VMH neuronal nuclei colored and labeled by cluster designation. (**D**) Mean scaled expression of marker genes across integrated clusters by species. (**E**) Proportion of cells in each cluster from the sample for each species (mean ± SEM). (**F**) Expression profile of the top enriched genes for each cluster. (**G**) Mapping of species-specific clusters onto the integrated clusters. (**H**) Species-specific ESμ for the top 3 marker genes for each integrated cluster determined by CELLEX.

Supplementary Figure Legends

Figure 1—figure supplement 1: Mouse snRNA-seq identifies major CNS classes. (**A**–**C**) The number of (**A**) cells, (**B**) genes, and (**C**) UMIs detected per sample used in this study after quality control. (**D**) UMAP projection of all 42,040 cells, colored by cluster. (**E**) Average percent of cells in each cluster across all samples. (**F**) Representative marker genes for each of the major CNS cell types. (**G**) Expression profile of top enriched genes for each cluster. (**H**) UMAP representation of cell type classification. (**I**) Quantification of cell classes per sample.

Figure 2—figure supplement 1: Comparison with VMH data from Kim et al. (**A**) UMAP projection of each dataset separately. Cells labeled "(Missing)" were present in the dataset, but were excluded from final VMH clustering. (**B**) Pair-wise expression correlation of variable genes for each cluster in each dataset. (**C**) UMAP projection of CCA-integrated data, colored by cluster. (**D**) Mean scaled expression of marker genes for each cluster. (**E**) UMAP projection of integrated data, by dataset of origin. (**F**) Breakdown of cluster designation from original dataset and integrated dataset.

Figure 2—figure supplement 2: Comparison of data with VMH data from Campbell et al. (**A**) UMAP projection of each dataset separately. (**B**) Pair-wise expression correlation of variable genes for each cluster in each dataset. (**C**) UMAP projection of CCA-integrated data, colored by cluster. (**D**) Mean scaled expression of marker genes for each cluster. (**E**) UMAP projection of integrated data, by dataset of origin. (**F**) Breakdown of cluster designation from original dataset and integrated dataset.

Figure 2—figure supplement 3: Identification of VMH neuronal "classes." The silhouette width for each cell for each level of VMH neuron classification. The mean silhouette width and the number of cells with a silhouette width greater than 0 are noted above the plot. Cells are colored by their cluster color in Fig. 2A.

Figure 2—figure supplement 4: *Dlk1* is expressed in neurons adjacent to the VMH. *Dlk1* expression in the UMAP projection of (**A**) all neurons (with the VMH neurons outlined) and (**B**) VMH neurons.

Figure 2—figure supplement 5: VMH *Nfib* population localizes to dorsomedial compartment. (**A**–**B**) *Nfia* marks (**B**) a subset of VMH^{Nfib} neurons but is also widely expressed in (**A**) non-neuronal populations in the VMH. (**C**) Representative image showing GFP-IR (green) and NFIA-IR (magenta) in $Nr5a1^{eGFP\text{-}L10a}$ (*Nr5a1-Cre*;$R26^{eGFP\text{-}L10a}$) mice; white arrowheads indicate colocalization. (**B**) *Slc17a8* is a marker for VMH^{Nfib} cells and (**D**) is expressed in the most dorosmedial VMH according to the Allen Brain Atlas *in situ* database.

Figure S2—figure supplement 6: Foxp2 population localizes to anterolateral ("tuberal") compartment. (**A**) Allen Brain Atlas *in situ* for *tdTomato* in $Nr5a1^{tdTomato}$ mice (*Nr5a1-Cre*;$R26^{LSL\text{-}tdTomato}$) shows widespread expression outside of the core VMH in an area referred to as the tuberal nucleus. (**B**) The VMH^{Foxp2} population is also marked by *Cdh7* and *Ust* expression. (**C**–**E**) Allen Brain Atlas *in situ* images for (**C**) *Foxp2*, (**D**) *Cdh7*, and (**E**) *Ust* show expression in the tuberal VMH. (**F**) Representative image showing the

distribution of GFP-IR (green) in Foxp2$^{eGFP-L10a}$ (*Foxp2*$^{Cre/+}$;*R26*$^{eGFP-L10a}$) mice in the tuberal region.

Figure 3—figure supplement 1: Comparison of different TRAP-seq approaches for identifying genes enriched in *Lepr* VMH cells. (**A**, **B**) Comparison of Lepr$^{eGFP-L10a}$ (*Lepr*^{Cre};*R26*$^{LSL-eGFP-L10a}$) of the whole hypothlalmus (Hypothalamus Cre), Lepr$^{eGFP-L10a}$ with targeted dissection of the VMH (VMH Cre), and using the dual Flp- and Cre-dependent RCFL$^{eGFP-L10a}$ with *Lepr*^{Cre};*Slc17a6*^{Flpo} mice (VMH Cre+Flp). (**A**) Enrichment of control genes in each dataset. (**B**) Enrichment of genes conferring neurochemical identity that are significantly enriched in any of the 3 datasets. Dark red diamonds signify genes that are significantly enriched in the Nr5a1$^{eGFP-L10a}$ TRAP-seq (presumptive VMH).

Figure 4—figure supplement 1: Macaque snRNA-seq identifies major CNS classes. (**A**–**C**) The number of (**A**) cells, (**B**) genes, and (**C**) UMIs detected per sample used in this study after quality control. (**D**–**E**) UMAP projection of all cells, colored by (**D**) sample and (**E**) cluster. (**F**) Average percent of cells in each cluster across all samples. (**G**) Representative marker genes for each of the major CNS cell types. (**H**) Expression profile of top 10 enriched genes for each cluster. (**I**) UMAP representation of cell type classification. (**J**) Quantification of cell classes per sample.

Figure 4—figure supplement 2: Identifying VMH neurons in macaque. (**A**) UMAP projection and labeling by cluster and (**B**) expression of top 10 genes for each macaque neuron cluster. (**C**) *FEZF1* and (**D**) NR5A1 expression across the macaque neurons. (**E**) Loading on the top enriched mouse *Nr5a1-Cre* TRAP-seq genes.

Figure 5—figure supplement 1: Similarities of mouse and macaque clusters. (**A**) Transferred cluster designations from mouse to macaque (and vice versa) using the Seurat CCA projection, colored by median transfer score with dot size corresponding to the number of cells from a given cluster transferred to each cluster. (**B**) Number of high confidence marker genes (CELLEX ESμ > 0.5) for each cluster and species. (**C**) Top

GO terms associated with genes common between the species. (**D**) Pairwise expression correlation of 4866 orthologous marker genes between mouse and macaque classes.

Figure 5—figure supplement 2: Cluster marker expression in macaque VMH. (**A**) (left column) Atlas image highlighting the region of interest and (other columns) representative fluorescent *in situ* hybridization images for *ACVR1C*, *LEPR*, and *SLC17A8* (all in green). (**B**) (left column) Expression of marker genes in the macaque VMH neurons, projected into UMAP space. (other columns) Representative images showing DAPI (blue) and fluorescent *in situ* hybridization for *ACVR1C* (red, top) or *SLC17A8* (red, bottom), *LEPR* (green), and merged images.

Supplementary File Legends

Supplementary File 1: $Nr5a1^{eGFP\text{-}L10a}$ VMH TRAP-seq enrichment results

Supplementary File 2: VMH pseudo-TRAP enrichment results

Supplementary File 3: ESμ values from CELLEX for each mouse VMH neuron cluster

Supplementary File 4: ESμ values from CELLEX for each mouse VMH neuron class

Supplementary File 5: $Lepr^{Slc17a6}$-L10a VMH TRAP-seq enrichment results

Supplementary File 6: VMH Lepr pseudo-TRAP enrichment results

Supplementary File 7: ESμ values from CELLEX for each macaque VMH neuron cluster

Supplementary File 8: ESμ values from CELLEX for each conserved VMH neuron cluster using combined data

Supplementary File 9: ESμ values from CELLEX for each conserved VMH neuron cluster using mouse data

Supplementary File 10: ESμ values from CELLEX for each conserved VMH neuron cluster using macaque data

A

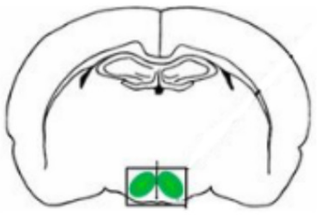

VMH dissection

nuclei isolation

10x sequencing

B

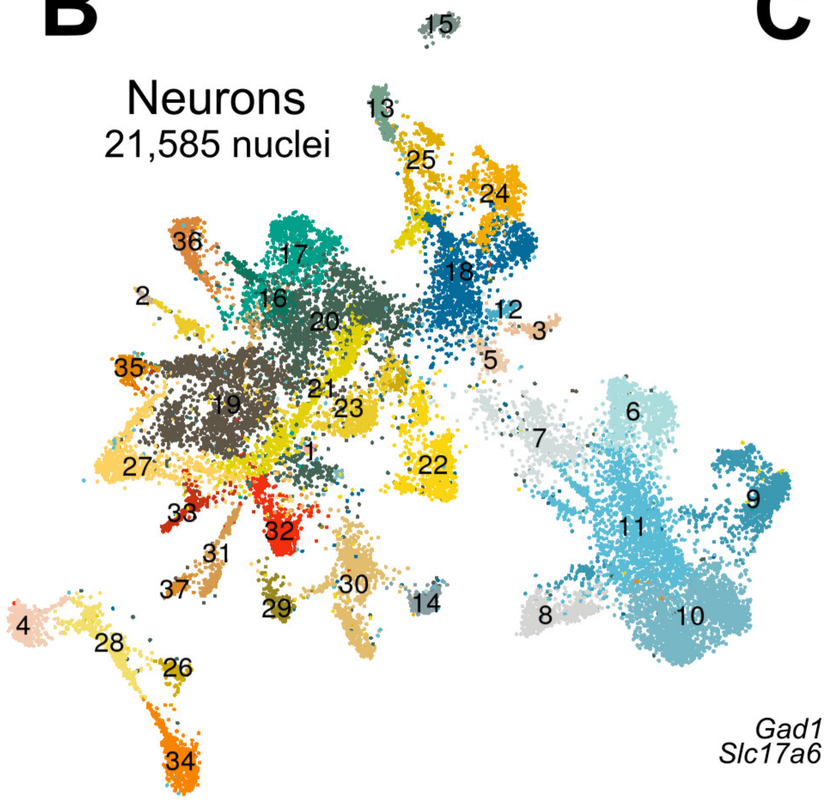

C

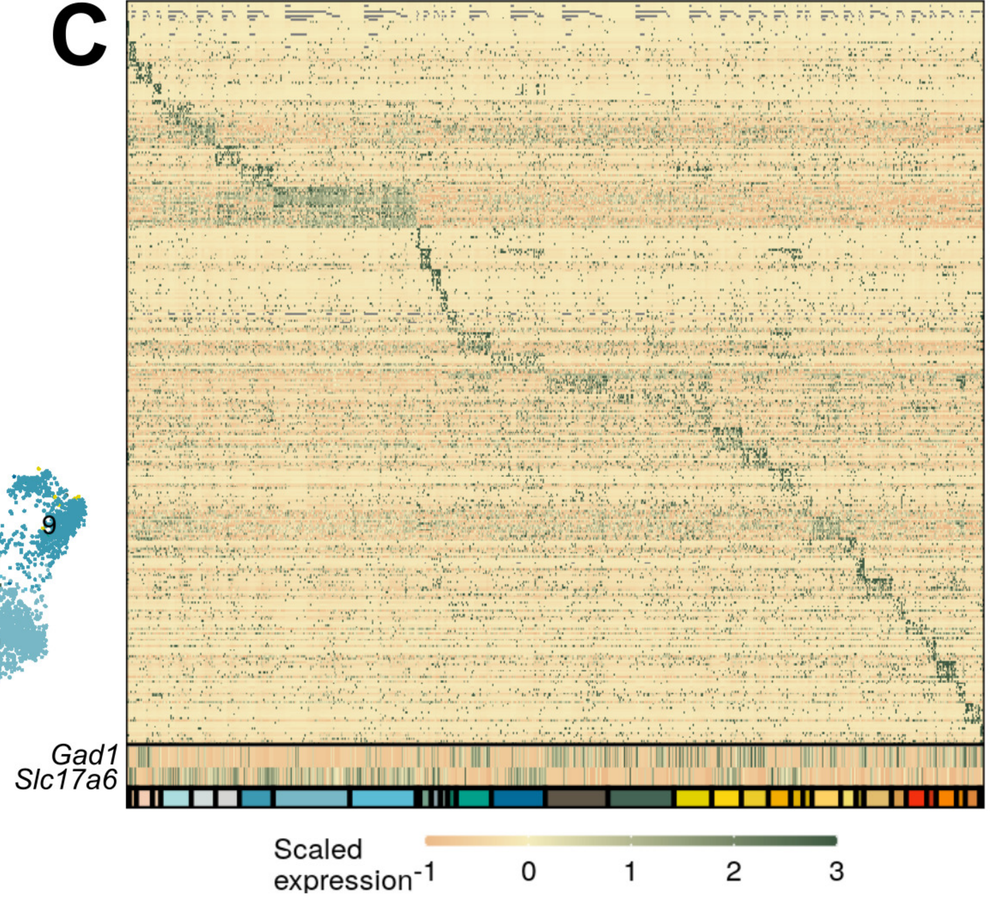

D

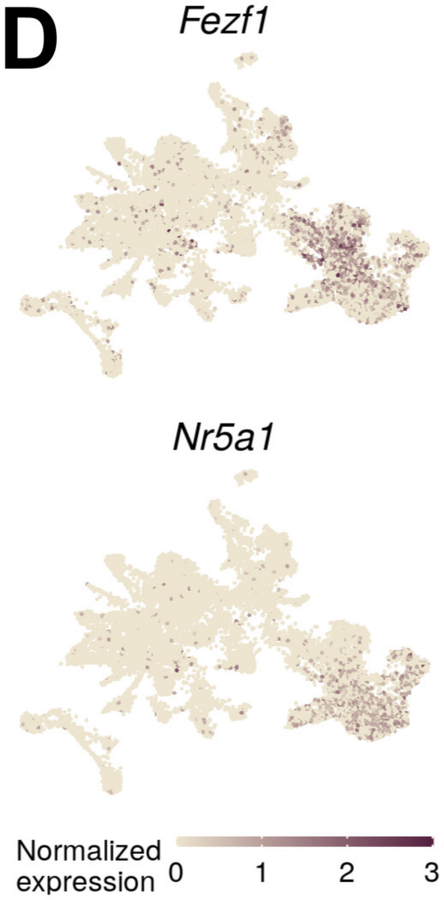

E

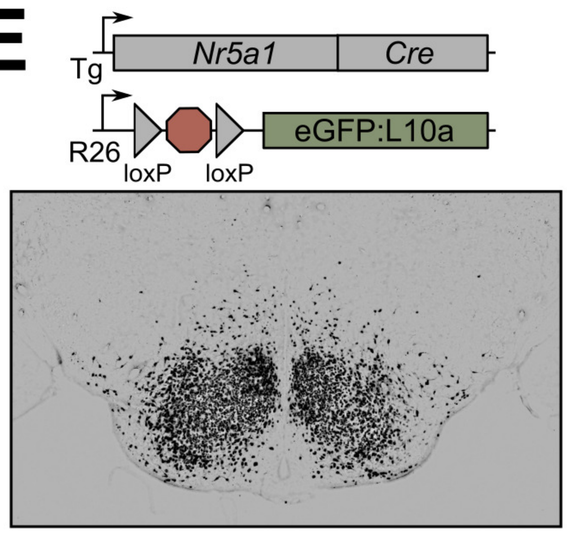

F

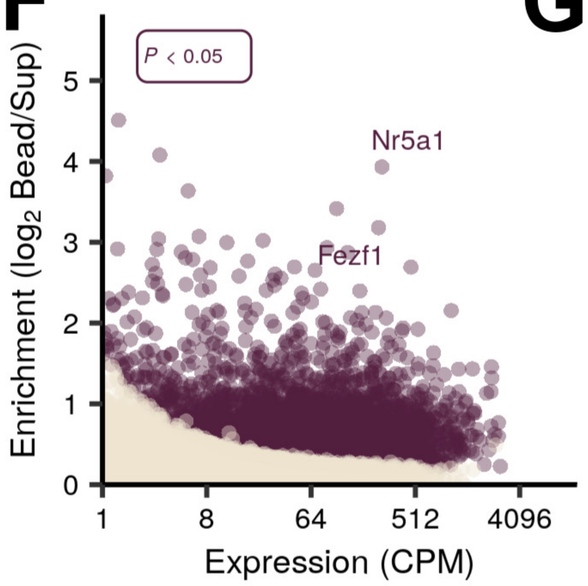

G

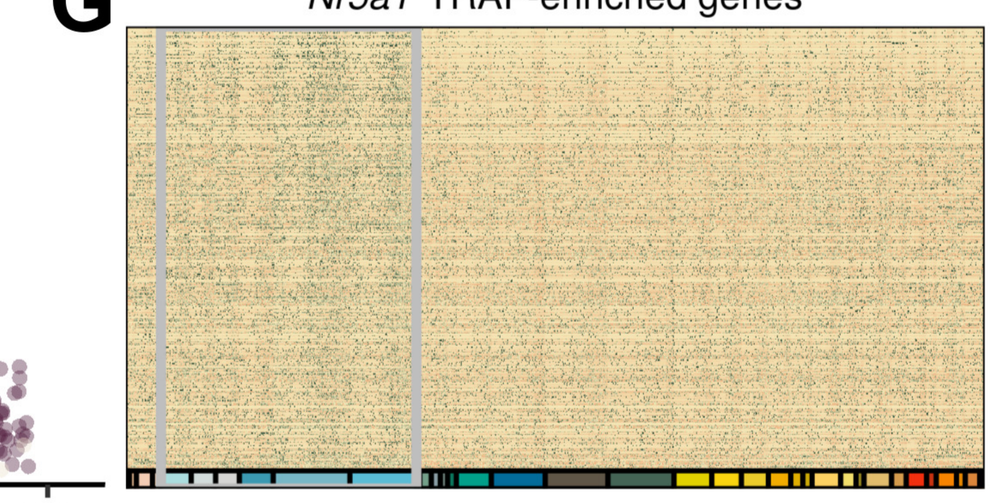

H

I

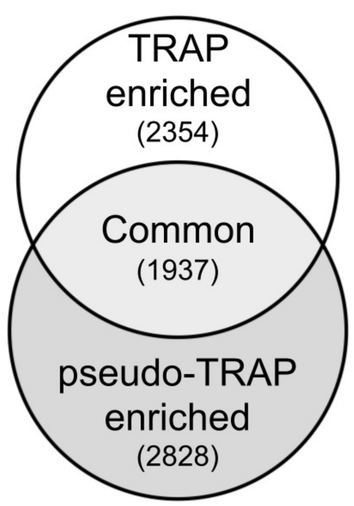

J

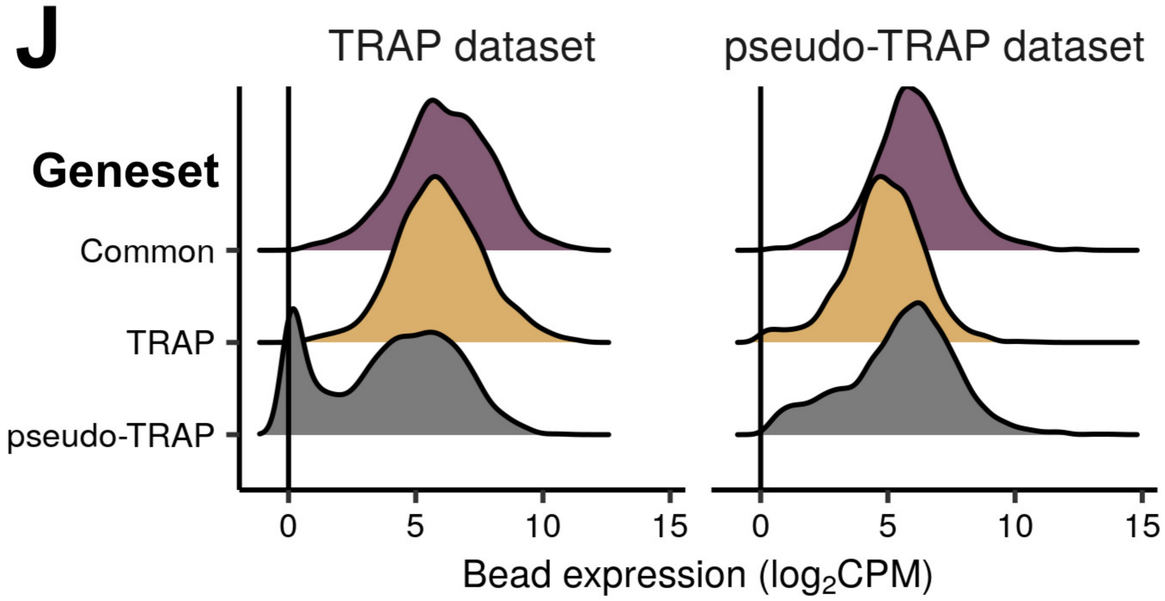

K

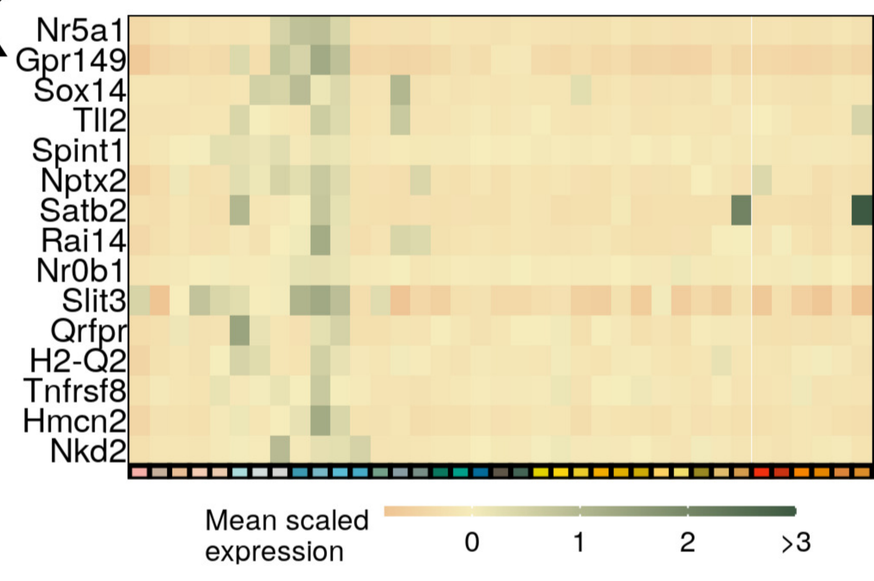

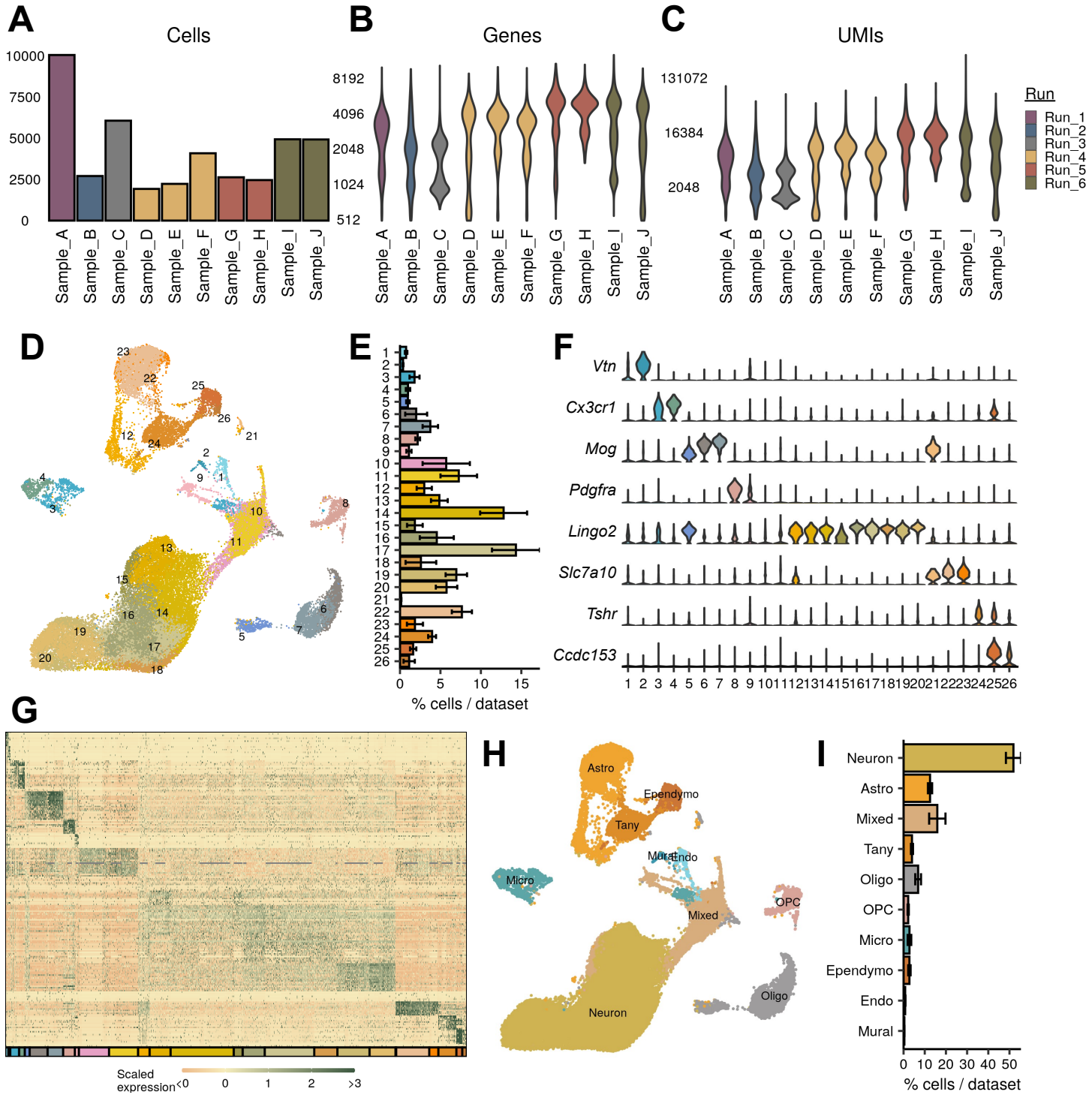
A
Cells
10000
7500
5000
2500
0
Sample_A
Sample_B
Sample_C
Sample_D
Sample_E
Sample_F
Sample_G
Sample_H
Sample_I
Sample_J
B
Genes
8192
4096
2048
1024
512
C
UMIs
131072
16384
2048
Run
Run_1
Run_2
Run_3
Run_4
Run_5
Run_6
D
E
% cells / dataset
F
Vtn
Cx3cr1
Mog
Pdgfra
Lingo2
Slc7a10
Tshr
Ccdc153
G
Scaled expression
<0
0
1
2
>3
H
Astro
Ependymo
Tany
Mural
Endo
Micro
Mixed
OPC
Oligo
Neuron
I
Neuron
Astro
Mixed
Tany
Oligo
OPC
Micro
Ependymo
Endo
Mural
% cells / dataset

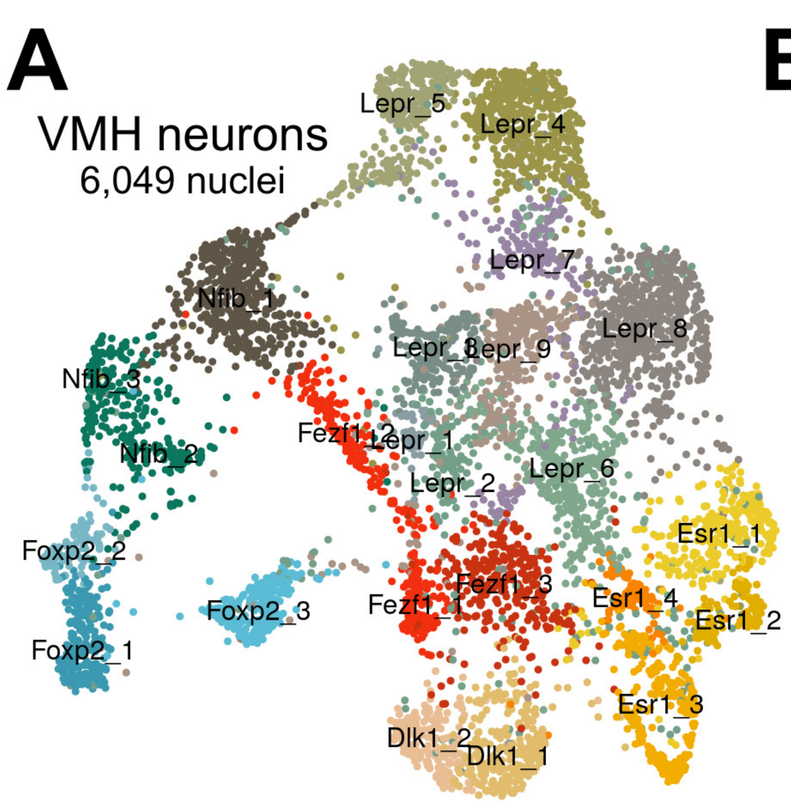
A
VMH neurons
6,049 nuclei
Lepr_5
Lepr_4
Lepr_7
Nfib_1
Lepr_8
Lepr_9
Nfib_3
Fezf1_2
Lepr_1
Nfib_2
Lepr_6
Lepr_2
Esr1_1
Foxp2_2
Fezf1_3
Esr1_4
Esr1_2
Foxp2_3
Fezf1_1
Foxp2_1
Esr1_3
Dlk1_2
Dlk1_1

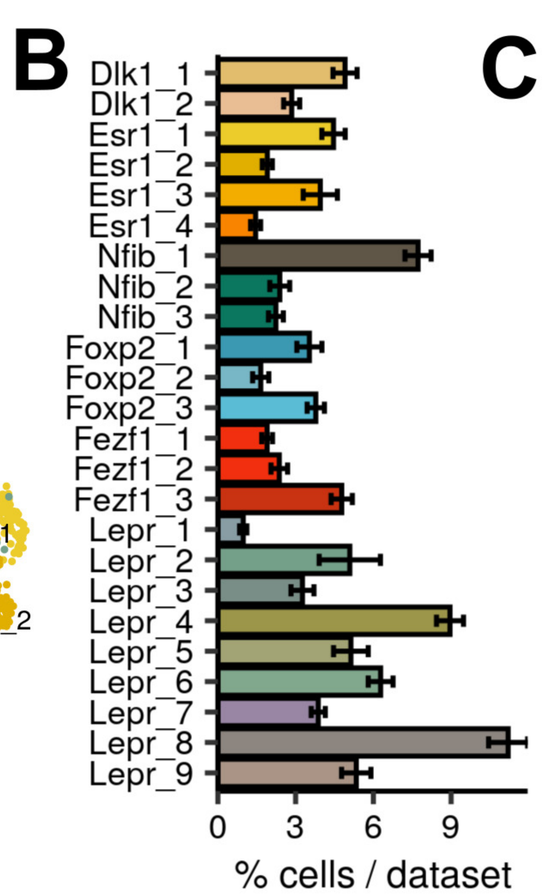
B
Dlk1_1
Dlk1_2
Esr1_1
Esr1_2
Esr1_3
Esr1_4
Nfib_1
Nfib_2
Nfib_3
Foxp2_1
Foxp2_2
Foxp2_3
Fezf1_1
Fezf1_2
Fezf1_3
Lepr_1
Lepr_2
Lepr_3
Lepr_4
Lepr_5
Lepr_6
Lepr_7
Lepr_8
Lepr_9
0
3
6
9
% cells / dataset

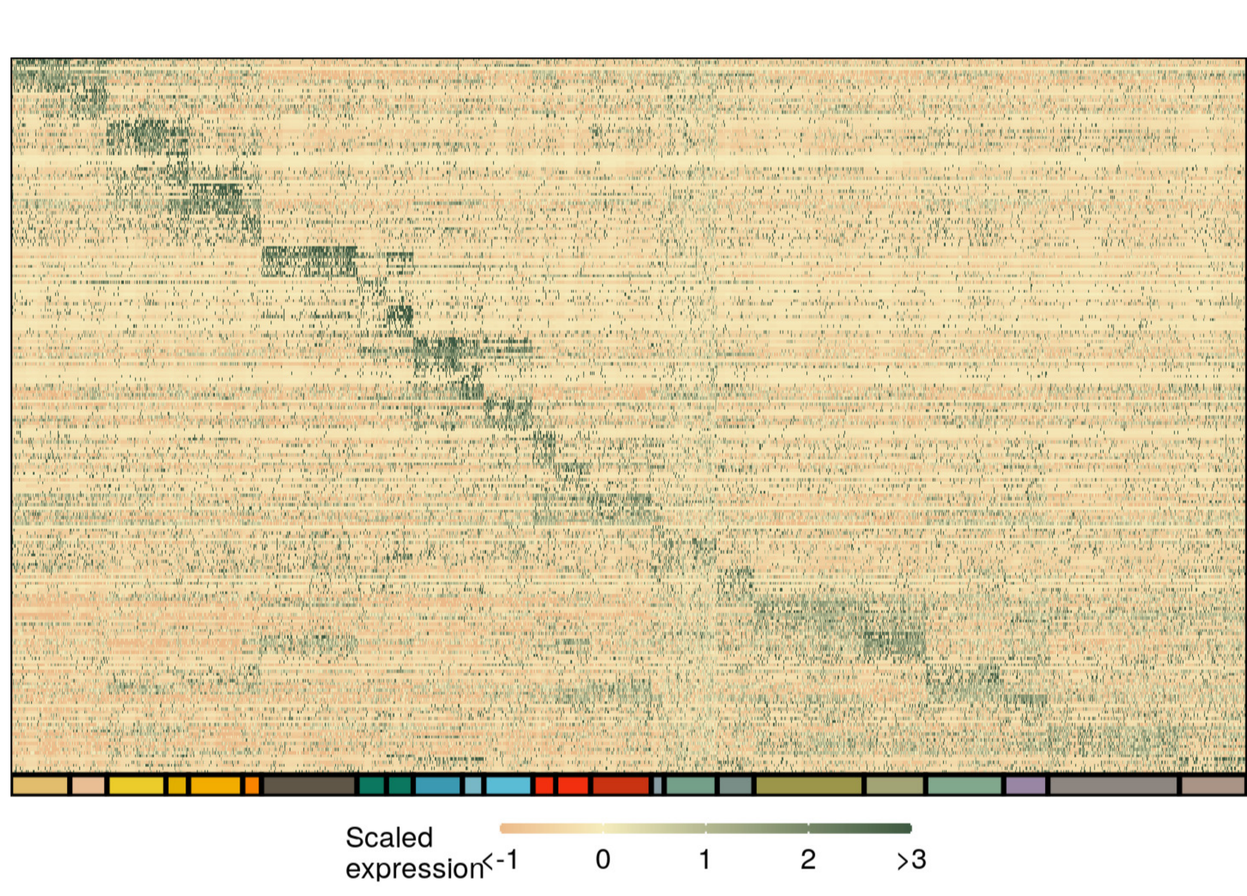
C
Scaled expression
<-1
0
1
2
>3

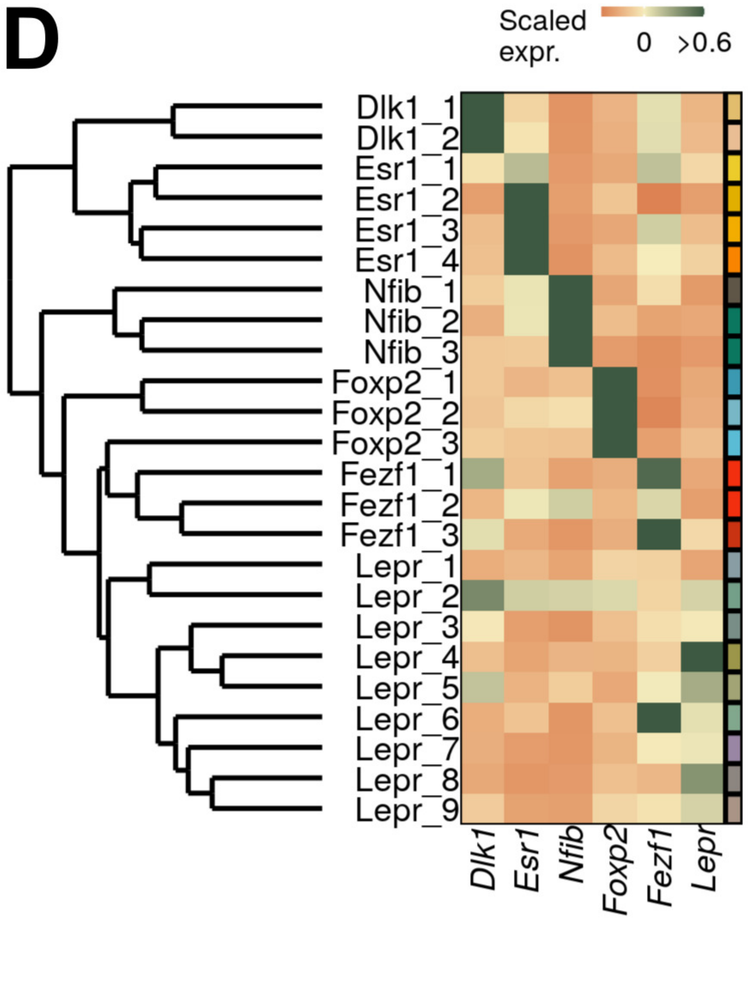
D
Scaled expr.
0
>0.6
Dlk1_1
Dlk1_2
Esr1_1
Esr1_2
Esr1_3
Esr1_4
Nfib_1
Nfib_2
Nfib_3
Foxp2_1
Foxp2_2
Foxp2_3
Fezf1_1
Fezf1_2
Fezf1_3
Lepr_1
Lepr_2
Lepr_3
Lepr_4
Lepr_5
Lepr_6
Lepr_7
Lepr_8
Lepr_9
Dlk1
Esr1
Nfib
Foxp2
Fezf1
Lepr

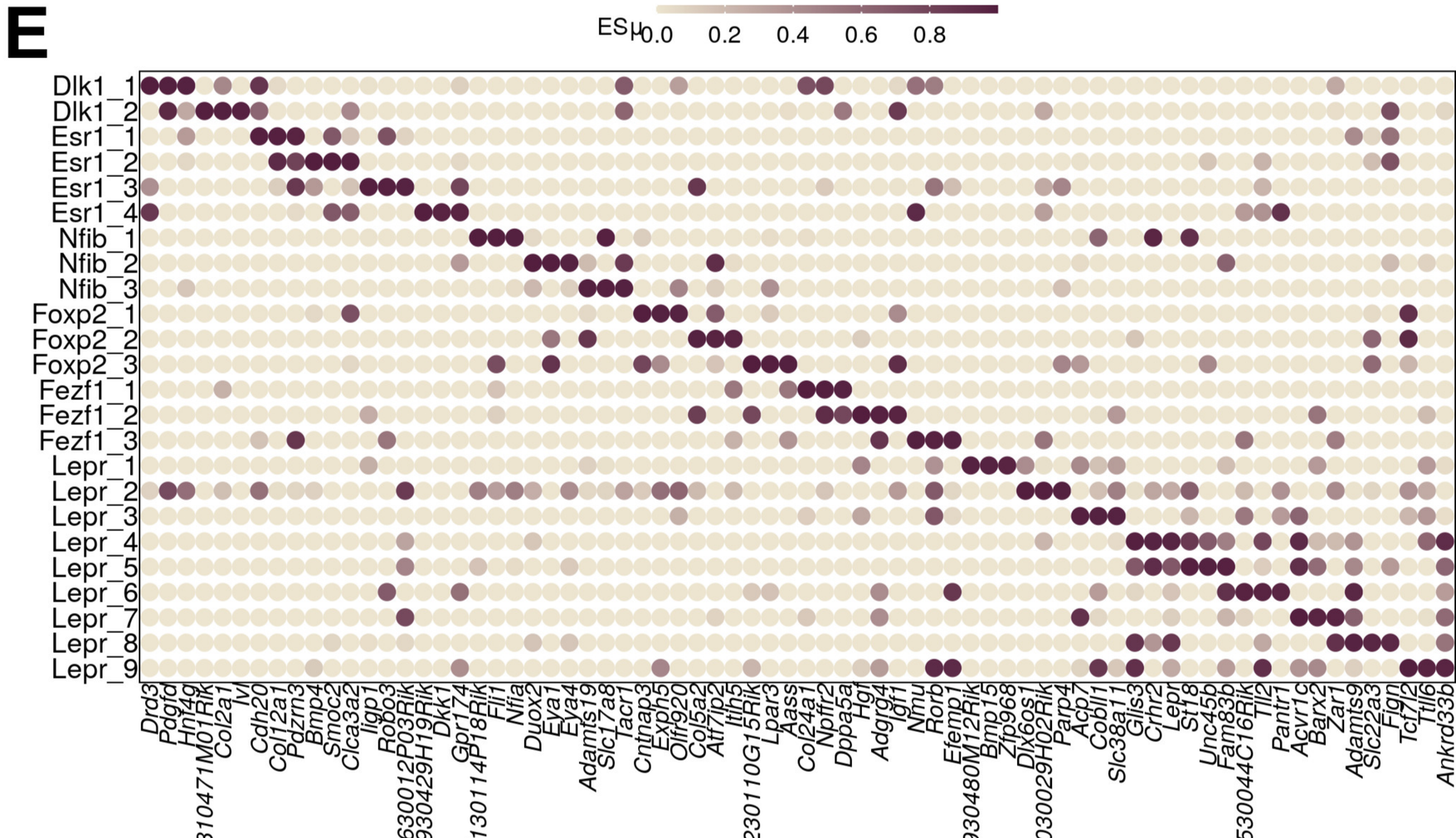
E
ESμ
0.0
0.2
0.4
0.6
0.8
Dlk1_1
Dlk1_2
Esr1_1
Esr1_2
Esr1_3
Esr1_4
Nfib_1
Nfib_2
Nfib_3
Foxp2_1
Foxp2_2
Foxp2_3
Fezf1_1
Fezf1_2
Fezf1_3
Lepr_1
Lepr_2
Lepr_3
Lepr_4
Lepr_5
Lepr_6
Lepr_7
Lepr_8
Lepr_9
Drd3
Pdgfd
Hn1g
2810471M01Rik
Col2a1
Ivl
Cdh20
Col12a1
Pdzrn3
Bmp4
Smoc2
Clca3a2
Iigp1
Robo3
A630012P03Rik
4930429H19Rik
Dkk1
Gpr174
E130114P18Rik
Fli1
Nfia
Duox2
Eya1
Eya4
Adamts19
Slc17a8
Tacr1
Cntnap3
Exph5
Olfr920
Col5a2
Atf7ip2
Itih5
B230110G15Rik
Lpar3
Aass
Col24a1
Npffr2
Dppa5a
Hgf
Adgrg4
Igf1
Nmu
Rorb
Efemp1
4930480M12Rik
Bmp15
Zfp968
Dlx6os1
C030029H02Rik
Parp4
Acp7
Cobll1
Slc38a11
Glis3
Crhr2
Lepr
St18
Unc45b
Fam83b
C530044C16Rik
Tll2
Pantr1
Acvr1c
Barx2
Zar1
Adamts9
Slc22a3
Flgn
Tcf7l2
Ttll6
Ankrd33b

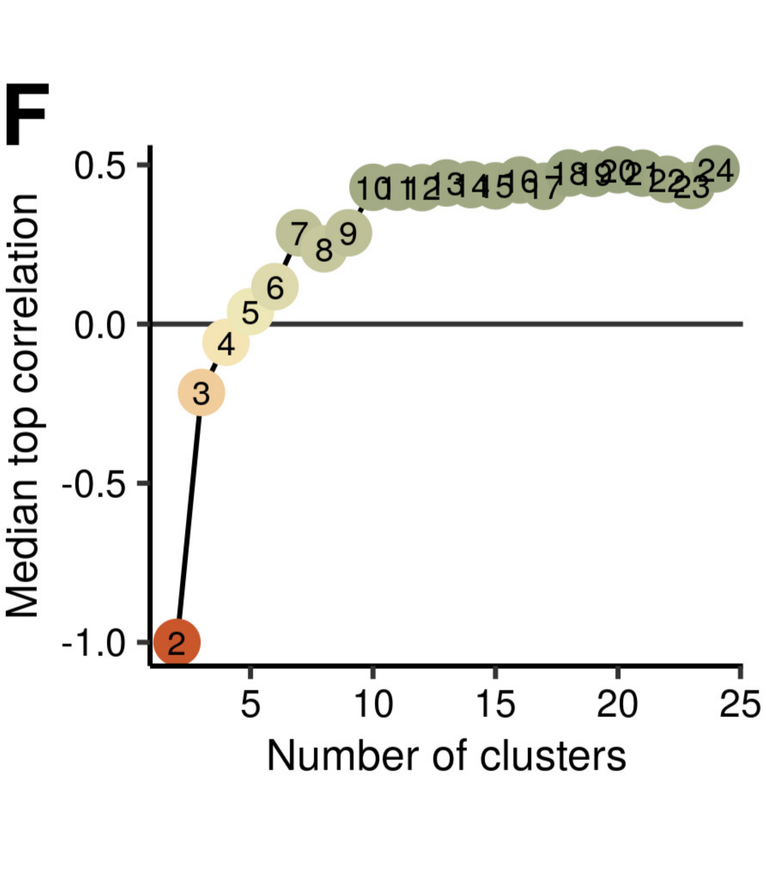
F
Median top correlation
0.5
0.0
-0.5
-1.0
1
2
3
4
5
6
7
8
9
10
11
12
13
14
15
16
17
18
19
20
21
22
23
24
5
10
15
20
25
Number of clusters

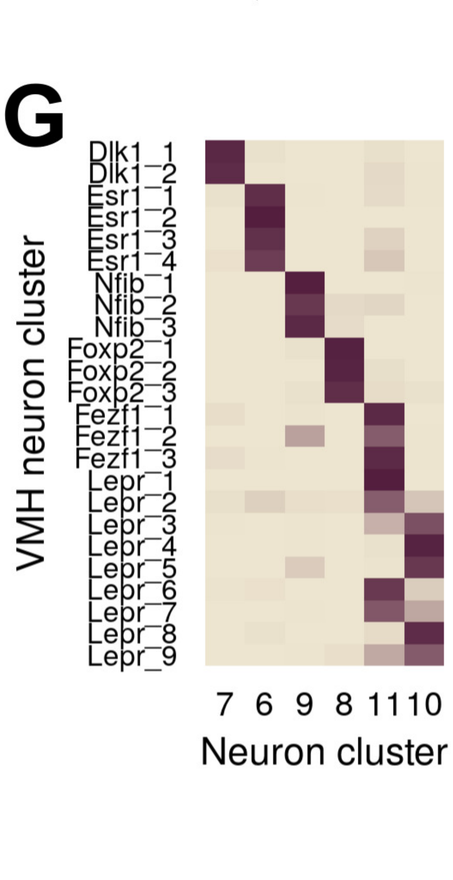
G
VMH neuron cluster
Dlk1_1
Dlk1_2
Esr1_1
Esr1_2
Esr1_3
Esr1_4
Nfib_1
Nfib_2
Nfib_3
Foxp2_1
Foxp2_2
Foxp2_3
Fezf1_1
Fezf1_2
Fezf1_3
Lepr_1
Lepr_2
Lepr_3
Lepr_4
Lepr_5
Lepr_6
Lepr_7
Lepr_8
Lepr_9
7
6
9
8
11
10
Neuron cluster
Percent
100
75
50
25
0

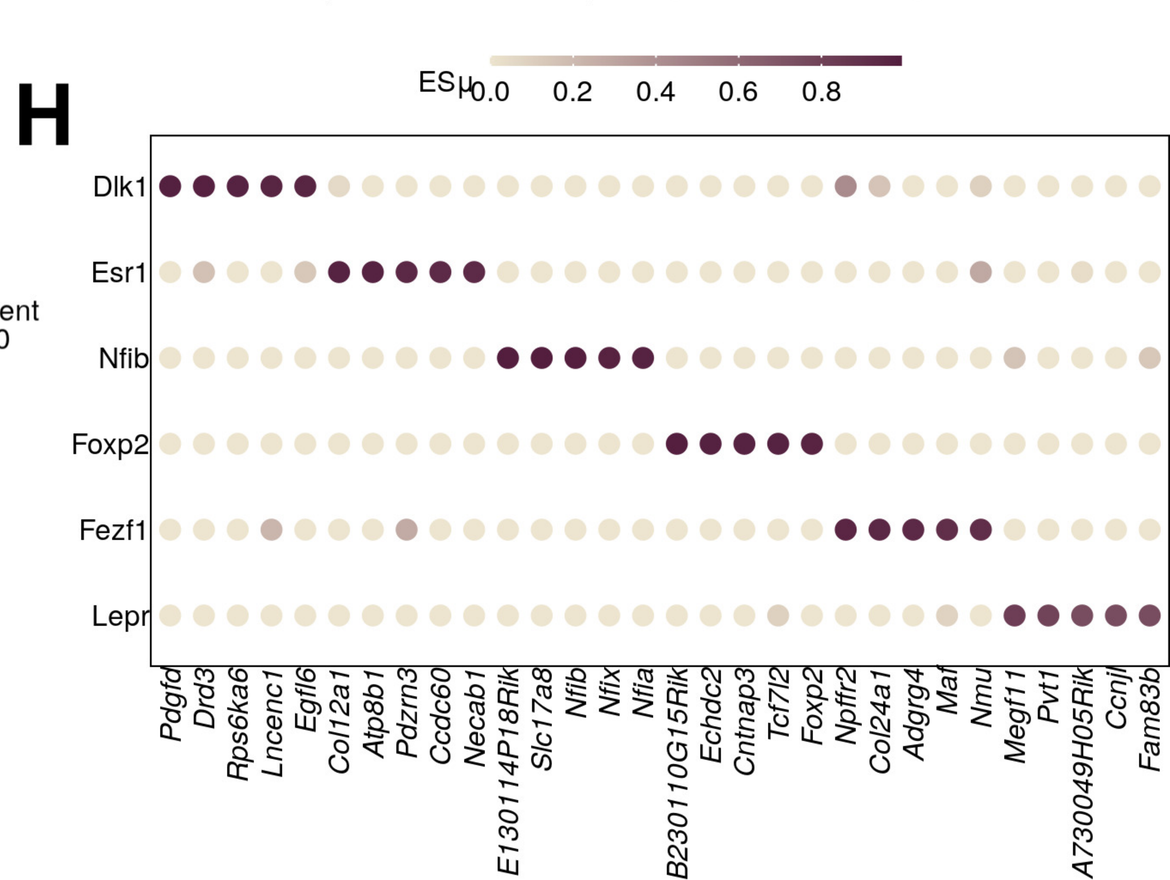
H
ESμ
0.0
0.2
0.4
0.6
0.8
Dlk1
Esr1
Nfib
Foxp2
Fezf1
Lepr
Pdgfd
Drd3
Rps6ka6
Lncenc1
Egfl6
Col12a1
Atp8b1
Pdzrn3
Ccdc60
Necab1
E130114P18Rik
Slc17a8
Nfib
Nfix
Nfia
B230110G15Rik
Echdc2
Cntnap3
Tcf7l2
Foxp2
Npffr2
Col24a1
Adgrg4
Maf
Nmu
Megf11
Pvt1
A730049H05Rik
Ccnjl
Fam83b

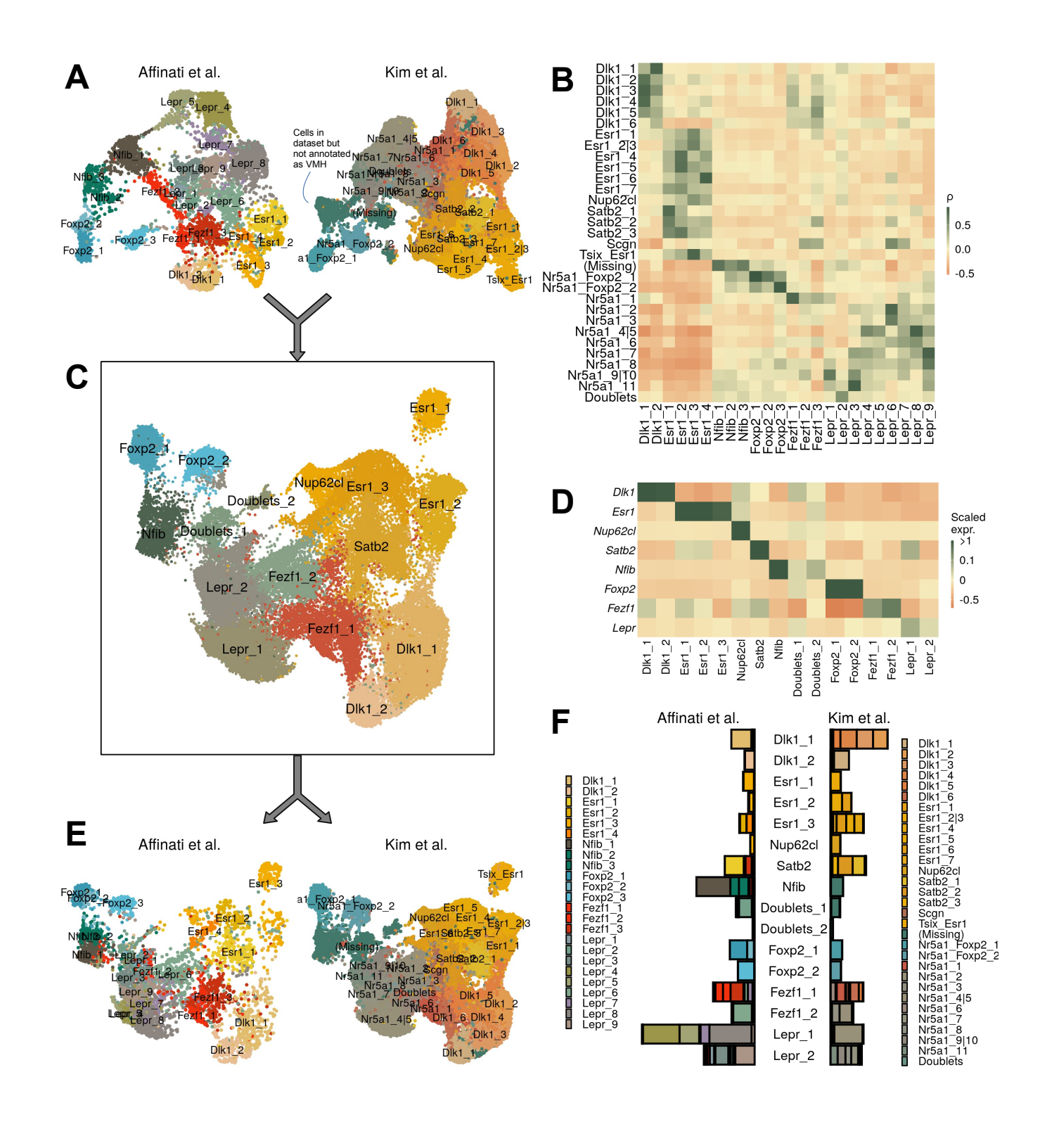
A
Affinati et al.
Kim et al.
Cells in dataset but not annotated as VMH
B
ρ
0.5
0.0
-0.5
C
D
Scaled expr.
>1
0.1
0
-0.5
E
Affinati et al.
Kim et al.
F
Affinati et al.
Kim et al.

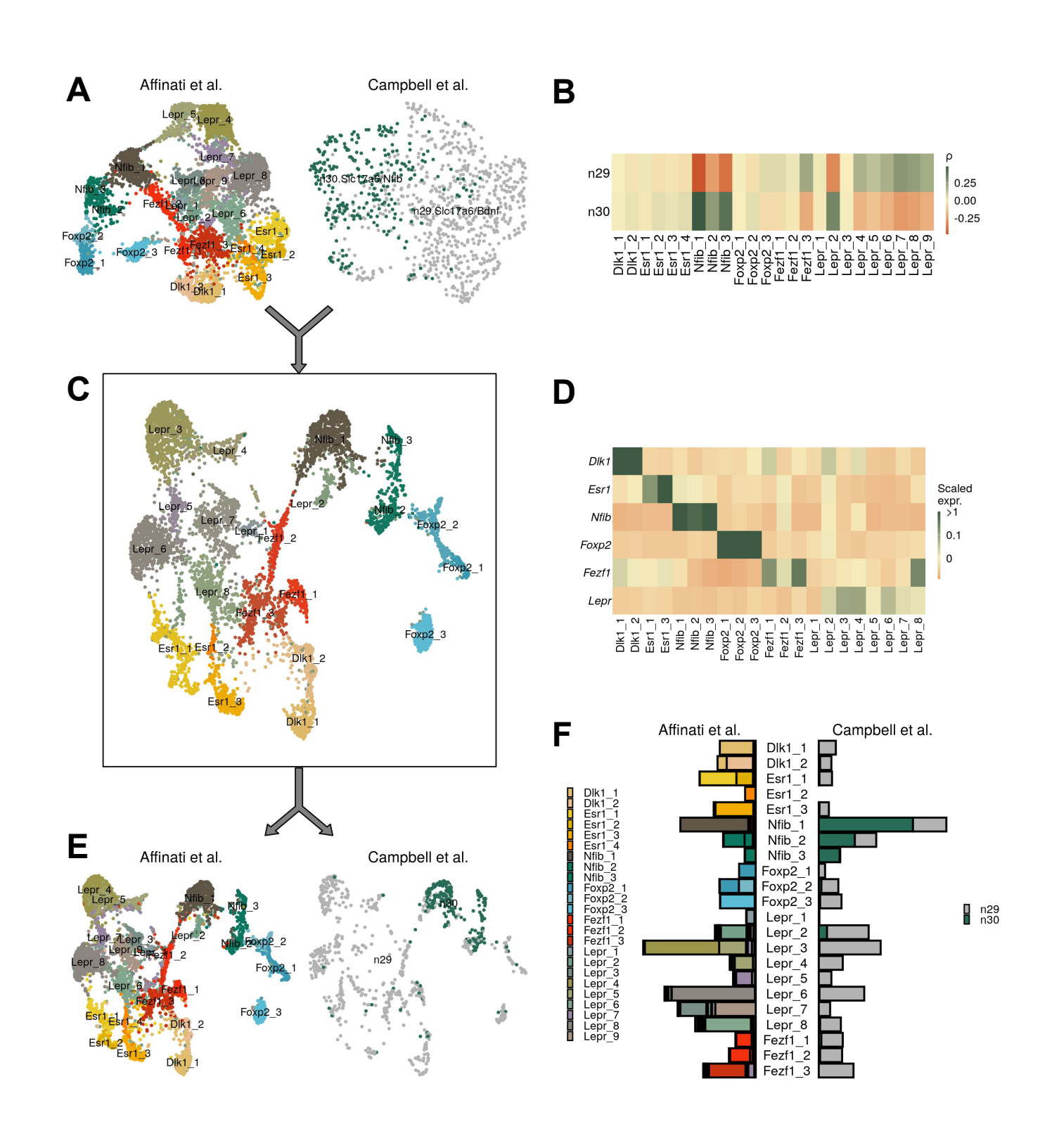
A
Affinati et al.
Campbell et al.
n30.Slc17a6/Nfib
n29.Slc17a6/Bdnf
B
n29
n30
ρ
0.25
0.00
-0.25
C
D
Dlk1
Esr1
Nfib
Foxp2
Fezf1
Lepr
Scaled expr.
>1
0.1
0
E
Affinati et al.
Campbell et al.
n30
n29
F
Affinati et al.
Campbell et al.
n29
n30

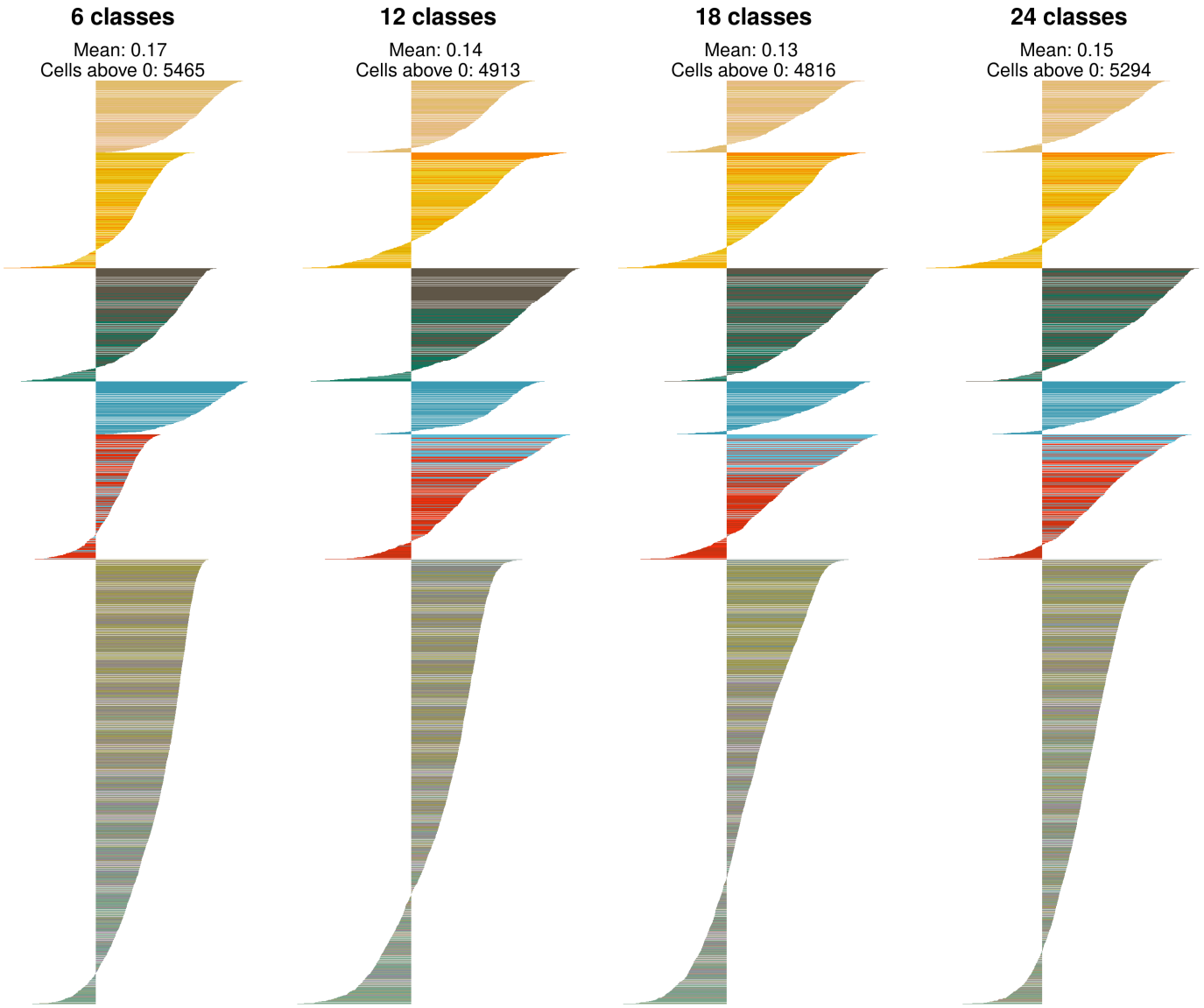
6 classes
Mean: 0.17
Cells above 0: 5465
12 classes
Mean: 0.14
Cells above 0: 4913
18 classes
Mean: 0.13
Cells above 0: 4816
24 classes
Mean: 0.15
Cells above 0: 5294

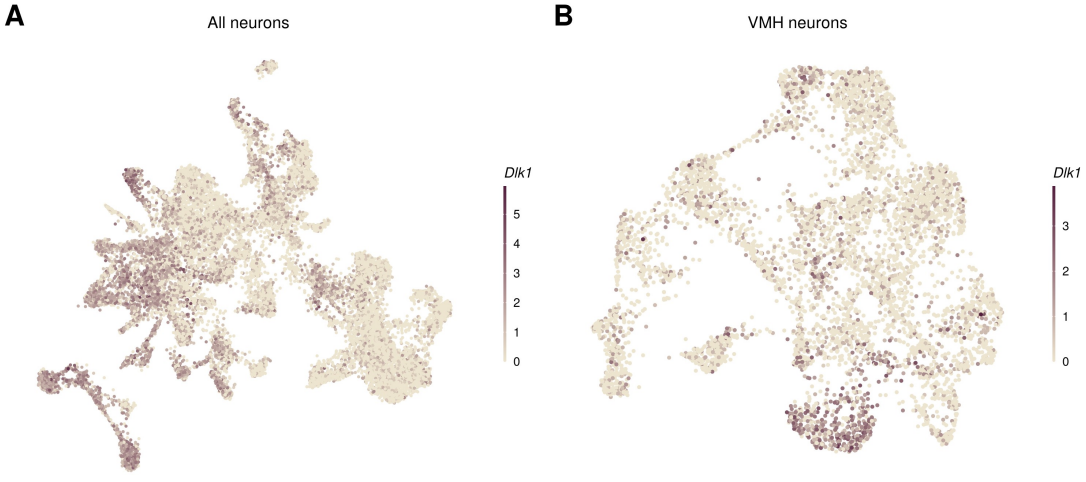
A
All neurons
Dlk1
5
4
3
2
1
0
B
VMH neurons
Dlk1
3
2
1
0

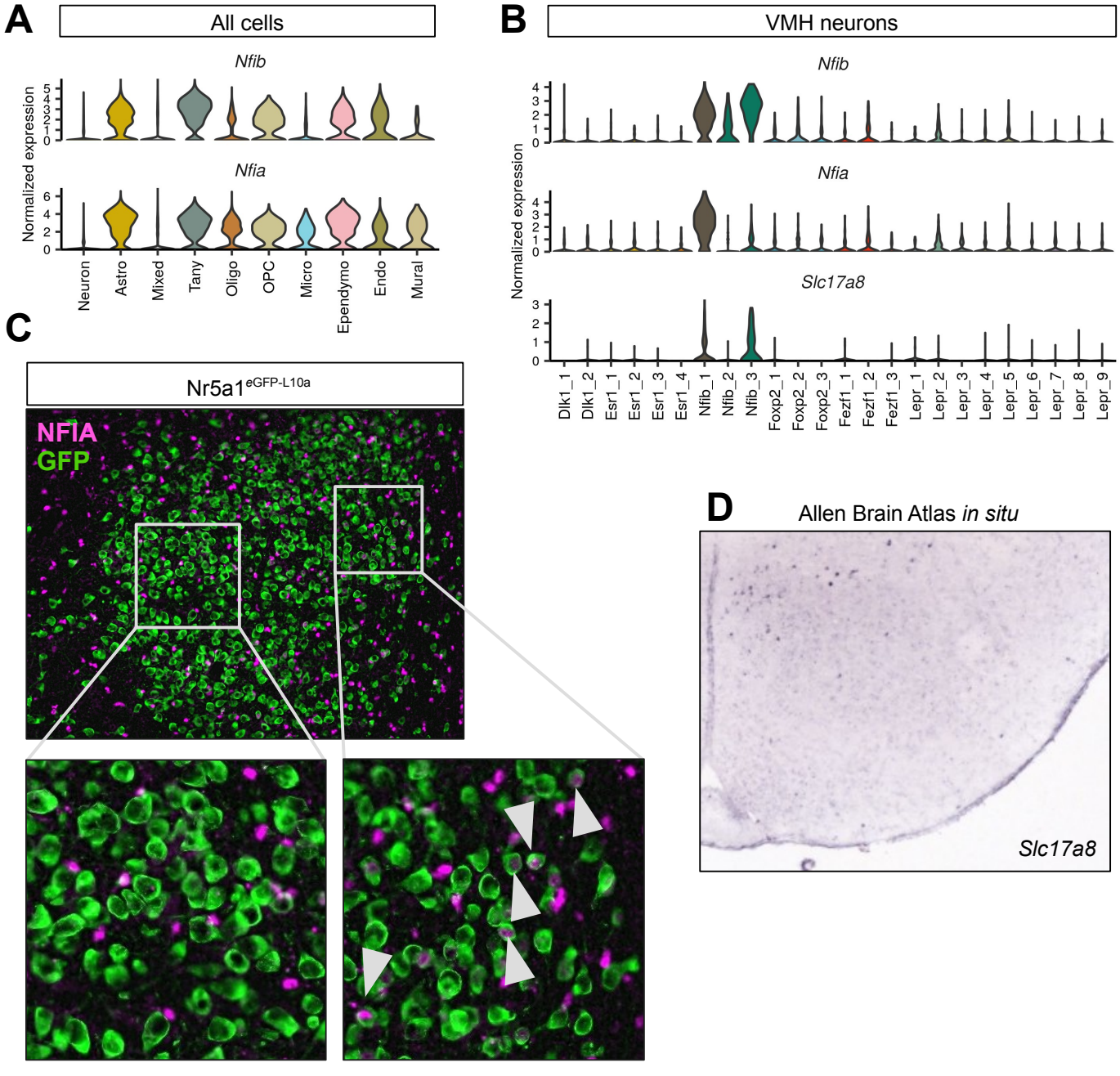
A
All cells
Nfib
Nfia
Normalized expression
Neuron
Astro
Mixed
Tany
Oligo
OPC
Micro
Ependymo
Endo
Mural
B
VMH neurons
Nfib
Nfia
Slc17a8
Normalized expression
Dlk1_1
Dlk1_2
Esr1_1
Esr1_2
Esr1_3
Esr1_4
Nfib_1
Nfib_2
Nfib_3
Foxp2_1
Foxp2_2
Foxp2_3
Fezf1_1
Fezf1_2
Fezf1_3
Lepr_1
Lepr_2
Lepr_3
Lepr_4
Lepr_5
Lepr_6
Lepr_7
Lepr_8
Lepr_9
C
Nr5a1eGFP-L10a
NFIA
GFP
D
Allen Brain Atlas in situ
Slc17a8

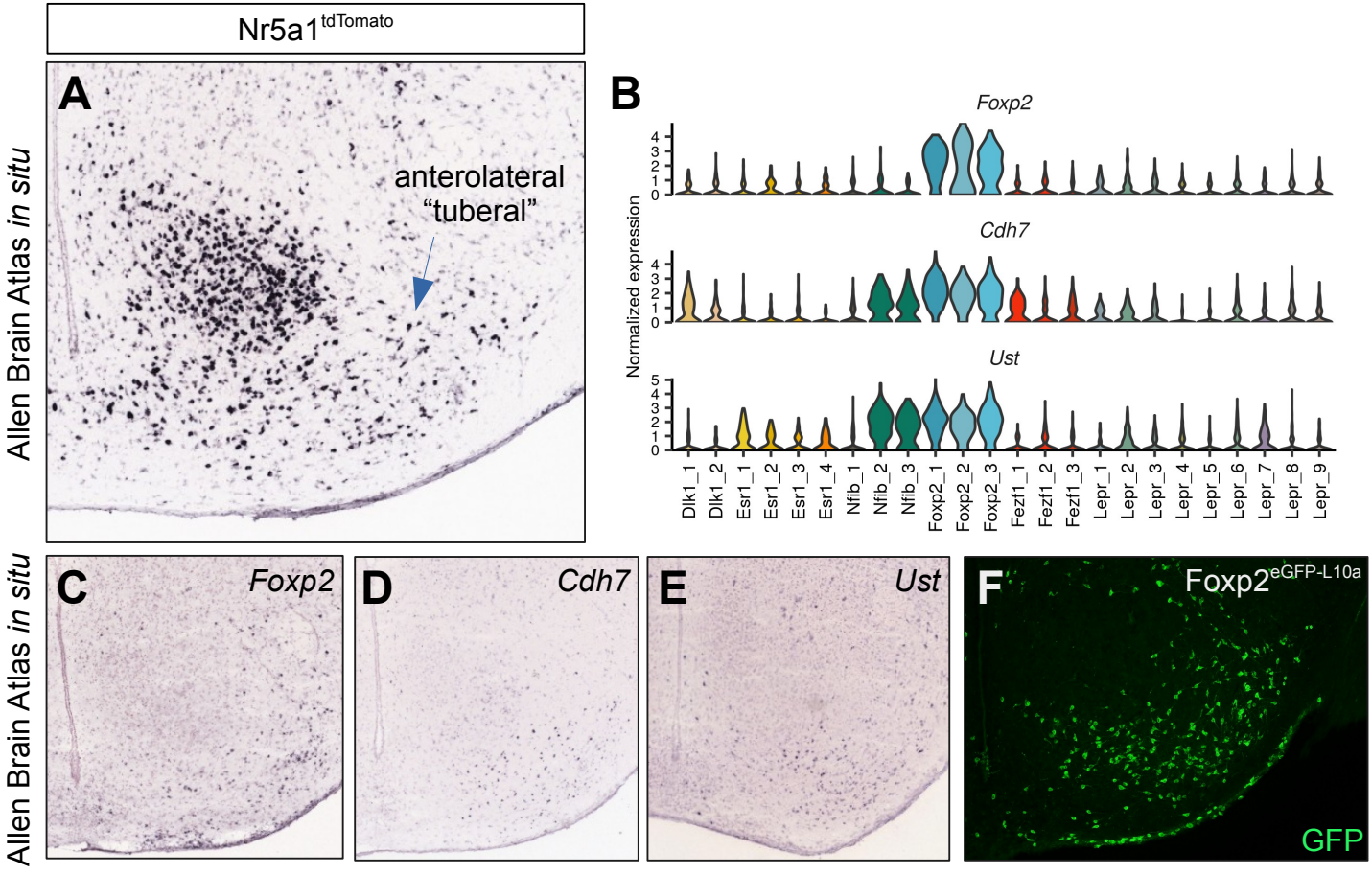
Nr5a1tdTomato
A
anterolateral
"tuberal"
Allen Brain Atlas in situ
B
Foxp2
Cdh7
Ust
Normalized expression
Dlk1_1
Dlk1_2
Esr1_1
Esr1_2
Esr1_3
Esr1_4
Nfib_1
Nfib_2
Nfib_3
Foxp2_1
Foxp2_2
Foxp2_3
Fezf1_1
Fezf1_2
Fezf1_3
Lepr_1
Lepr_2
Lepr_3
Lepr_4
Lepr_5
Lepr_6
Lepr_7
Lepr_8
Lepr_9
Allen Brain Atlas in situ
C
Foxp2
D
Cdh7
E
Ust
F
Foxp2eGFP-L10a
GFP

A

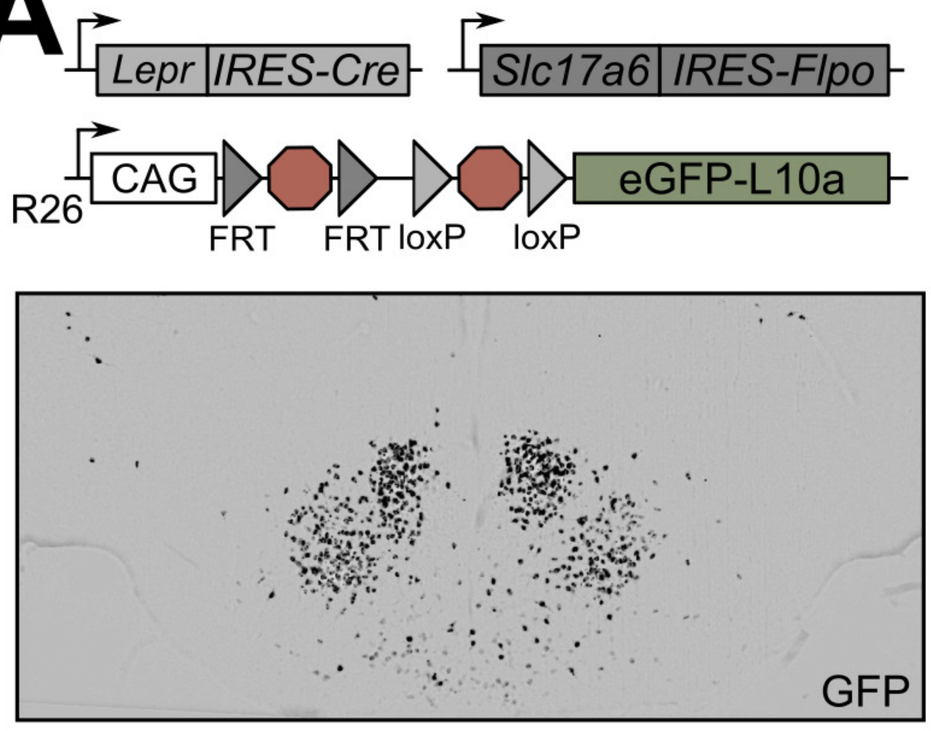

B

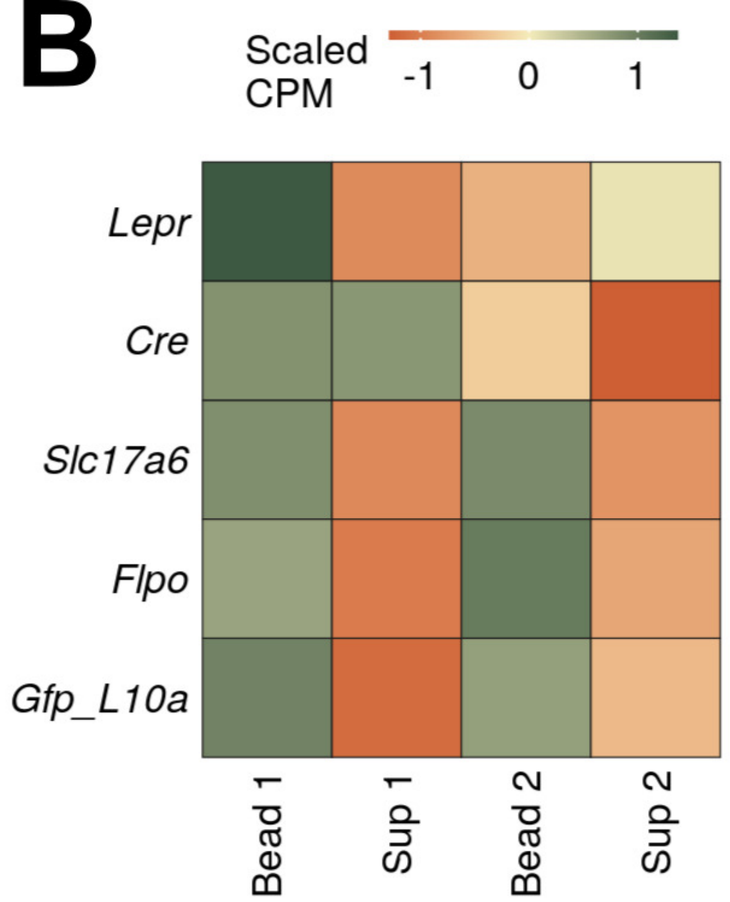

C

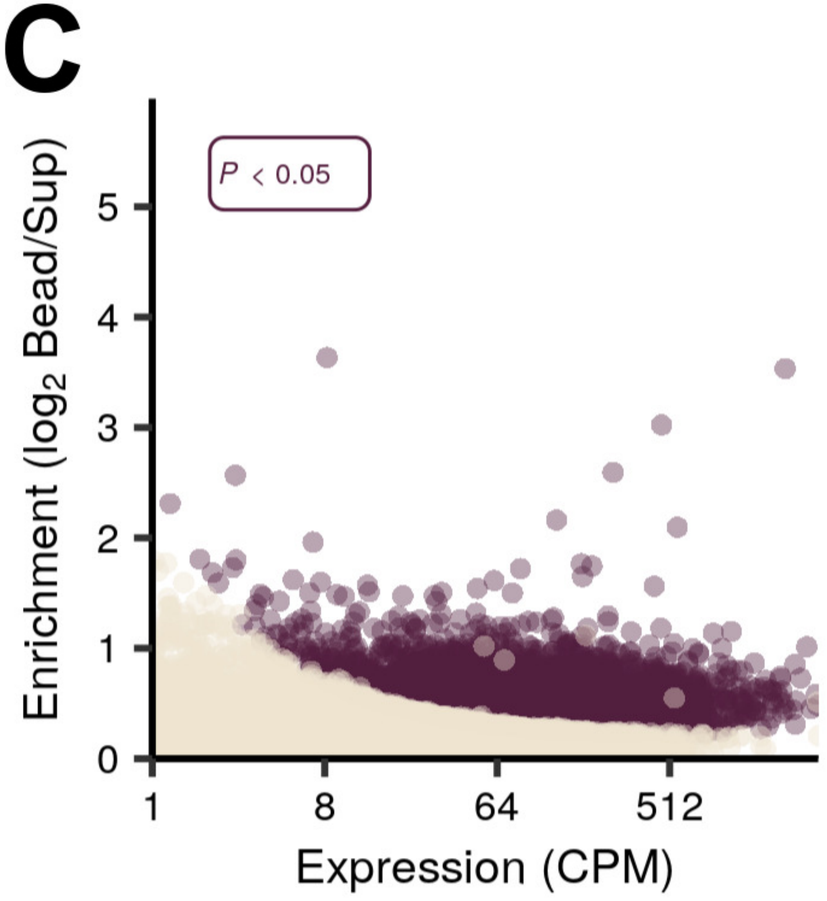

D

E

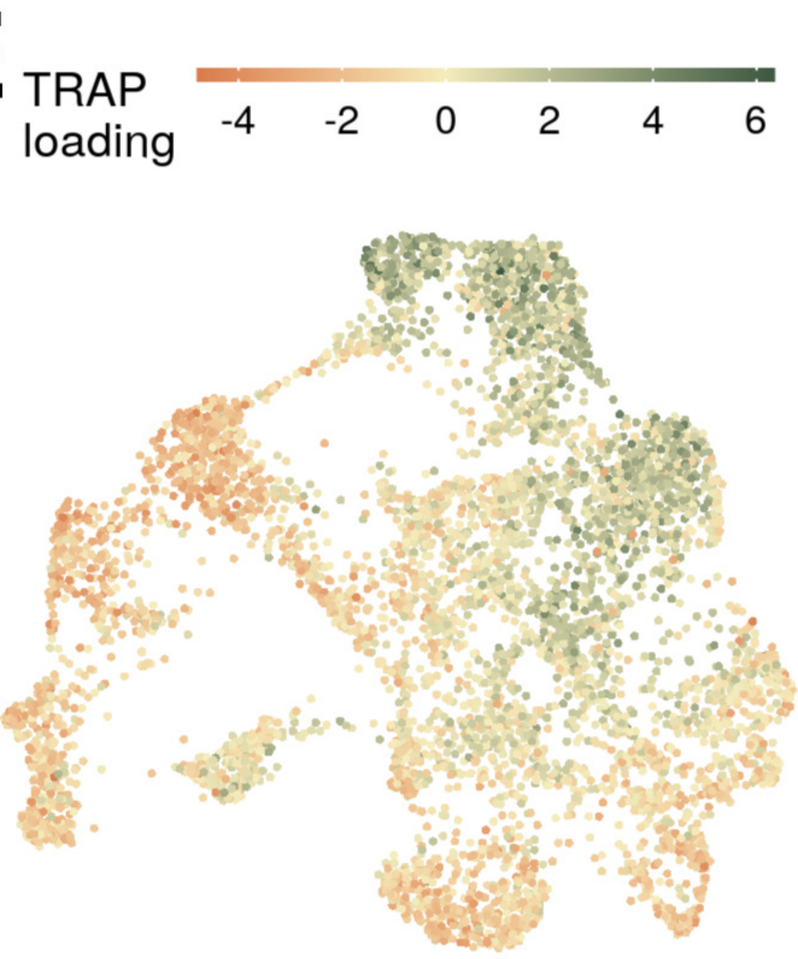

F

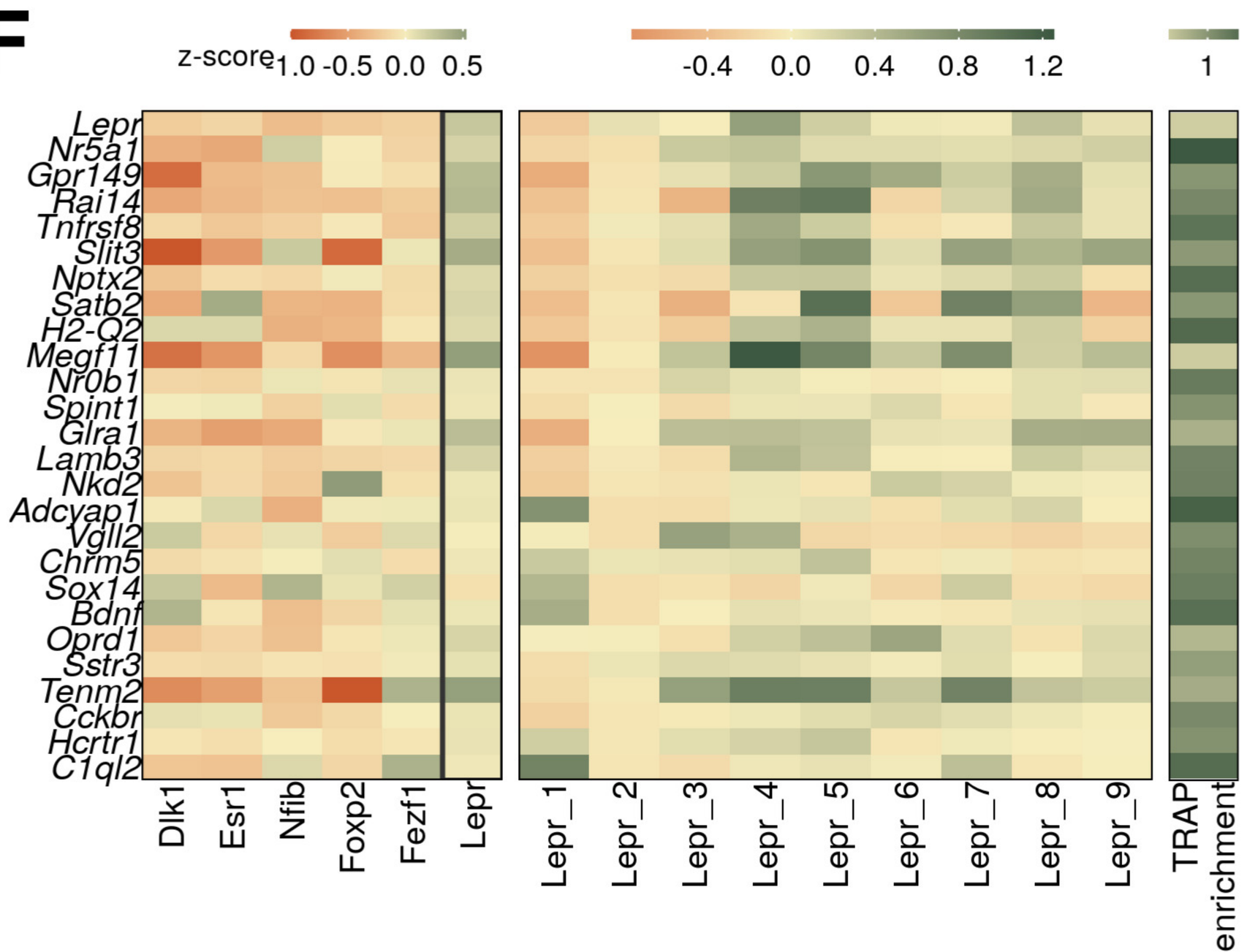

Allen Brain Atlas *in situ*

G

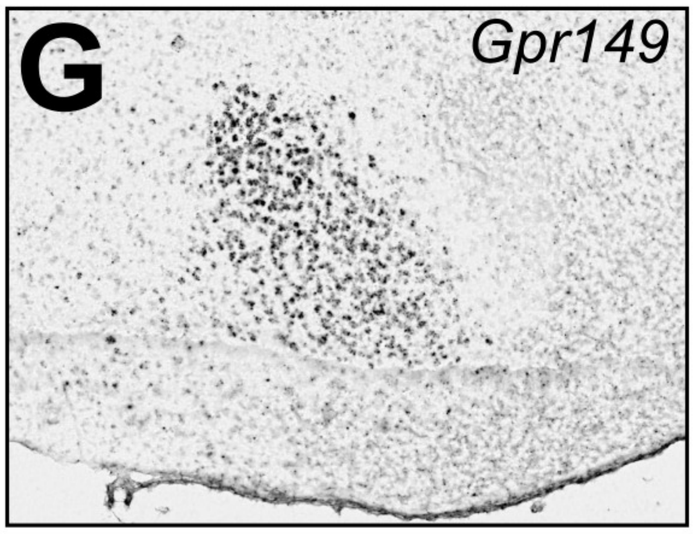

H

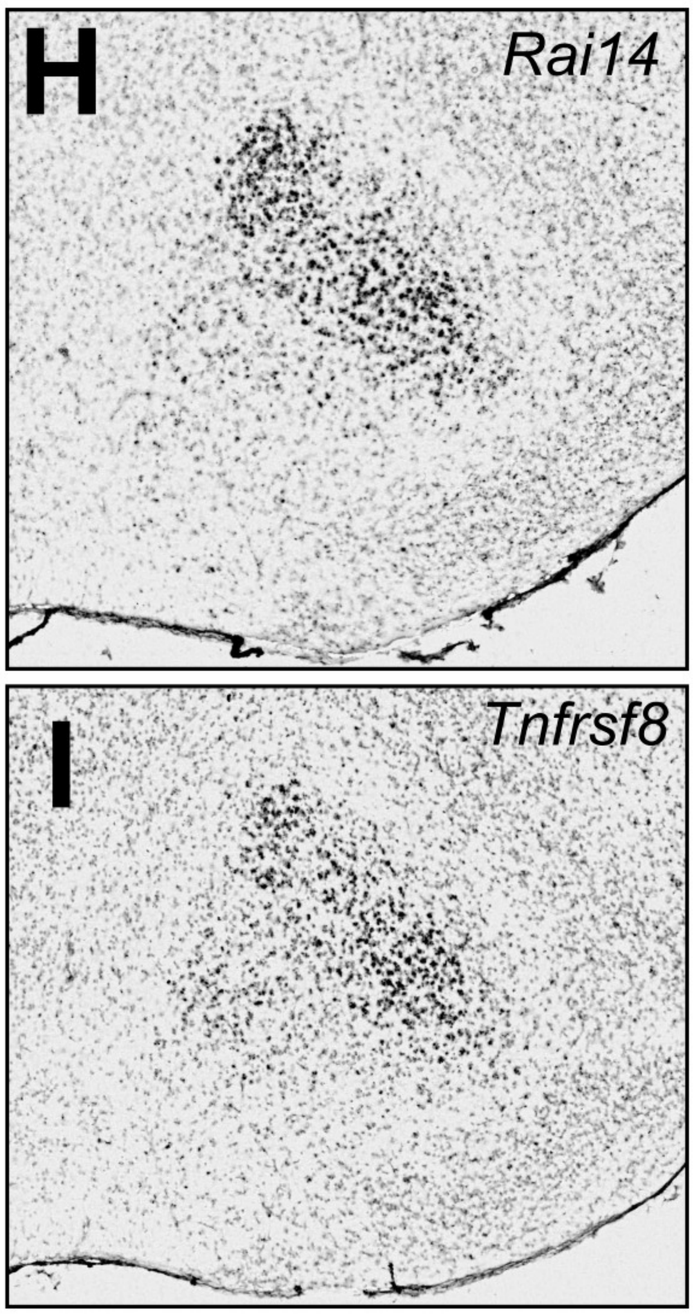

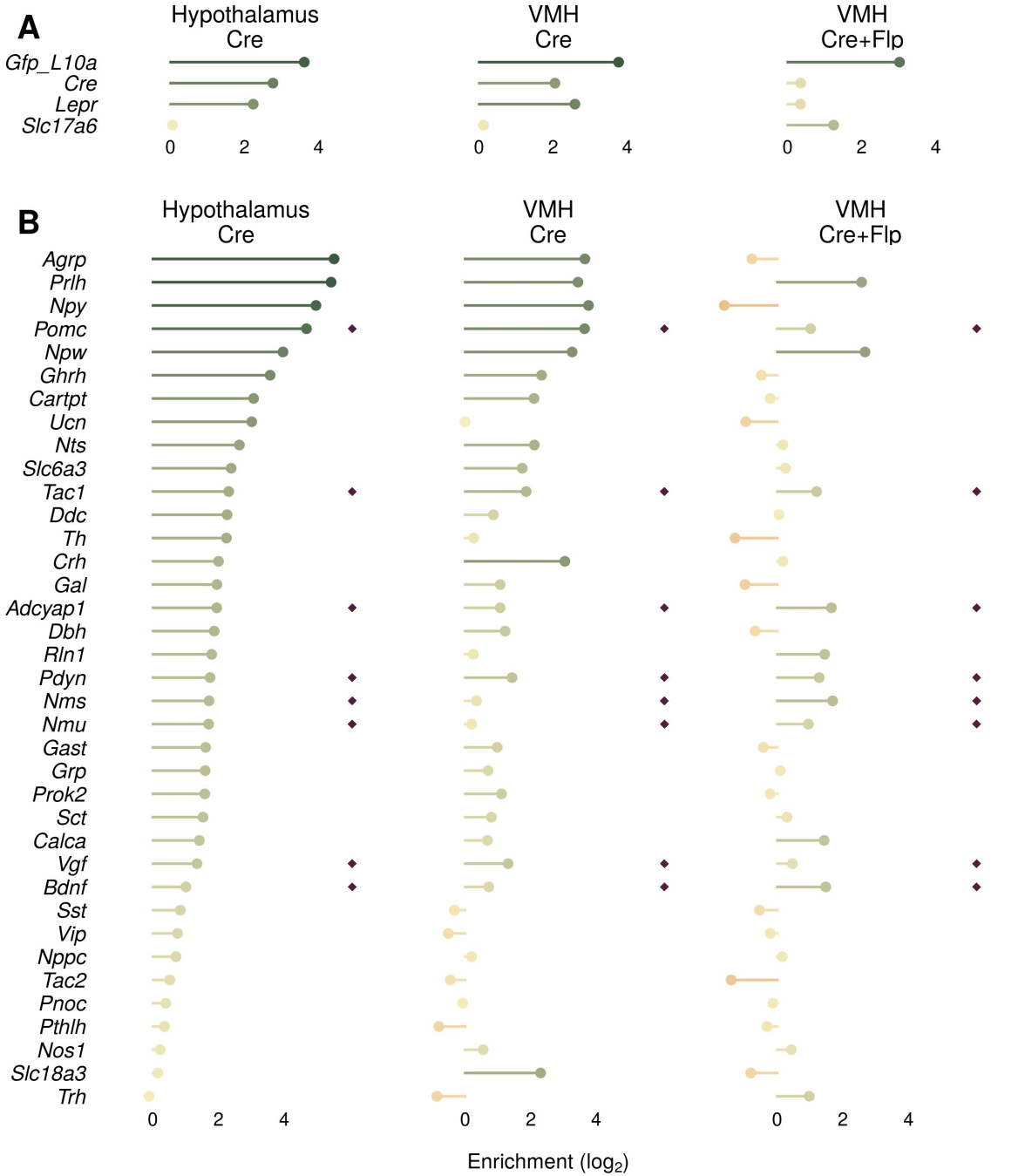
A
Hypothalamus Cre
VMH Cre
VMH Cre+Flp
Gfp_L10a
Cre
Lepr
Slc17a6
0
2
4
B
Hypothalamus Cre
VMH Cre
VMH Cre+Flp
Agrp
Prlh
Npy
Pomc
Npw
Ghrh
Cartpt
Ucn
Nts
Slc6a3
Tac1
Ddc
Th
Crh
Gal
Adcyap1
Dbh
Rln1
Pdyn
Nms
Nmu
Gast
Grp
Prok2
Sct
Calca
Vgf
Bdnf
Sst
Vip
Nppc
Tac2
Pnoc
Pthlh
Nos1
Slc18a3
Trh
Enrichment (log2)

A

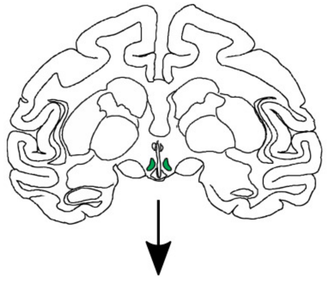

VMH dissection

nuclei isolation

10x sequencing

B

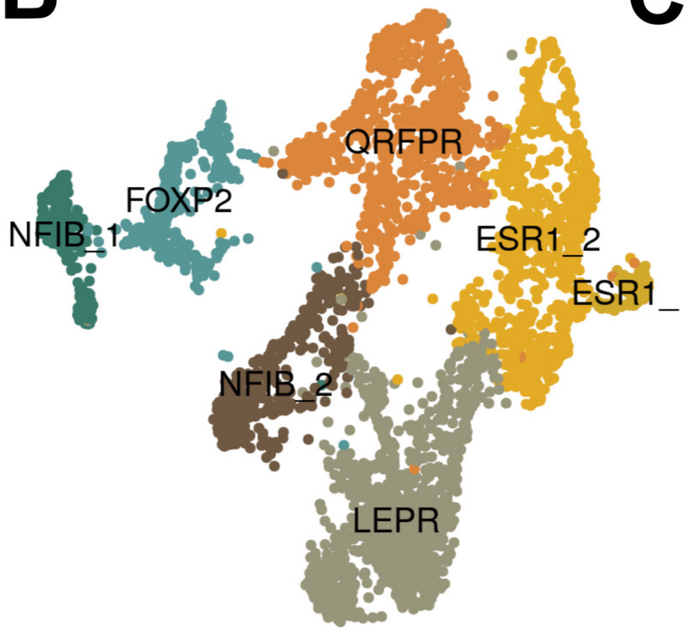

C

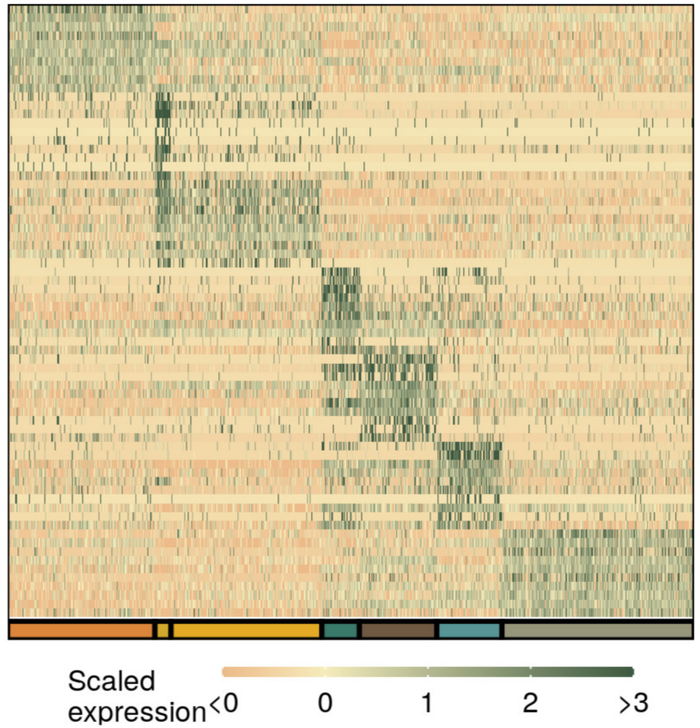

D

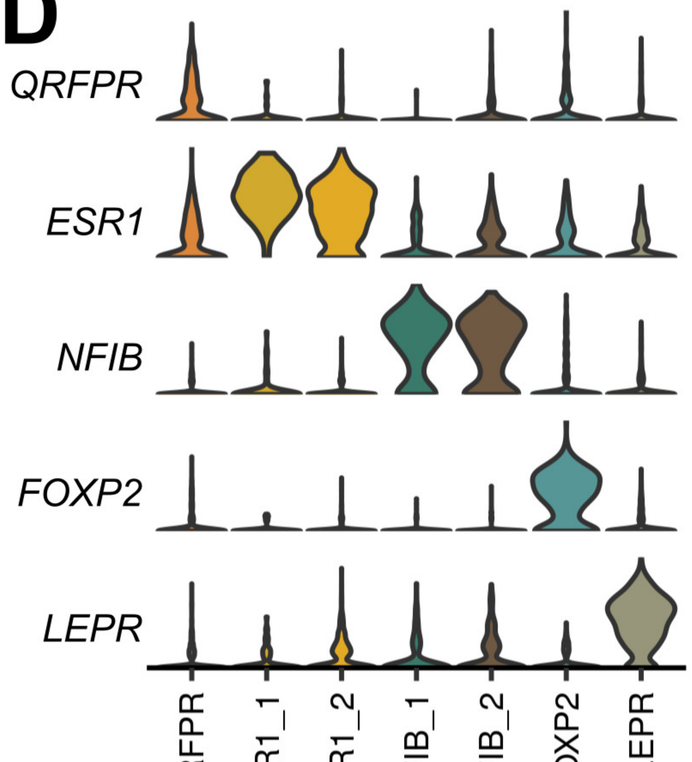

E

F

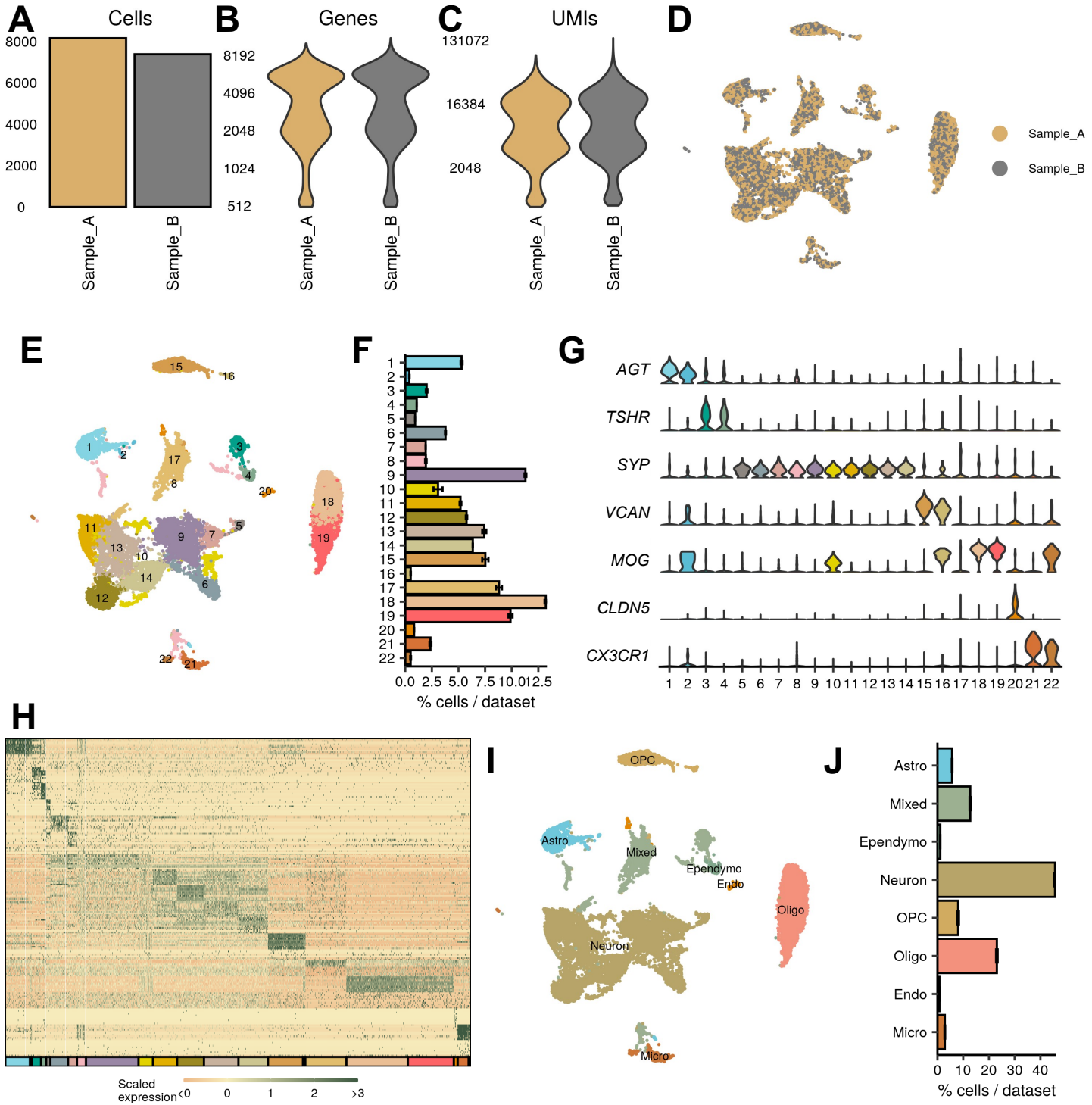
A
Cells
8000
6000
4000
2000
0
Sample_A
Sample_B
B
Genes
8192
4096
2048
1024
512
Sample_A
Sample_B
C
UMIs
131072
16384
2048
Sample_A
Sample_B
D
Sample_A
Sample_B
E
F
% cells / dataset
G
AGT
TSHR
SYP
VCAN
MOG
CLDN5
CX3CR1
H
Scaled expression
I
OPC
Astro
Mixed
Ependymo
Endo
Oligo
Neuron
Micro
J
Astro
Mixed
Ependymo
Neuron
OPC
Oligo
Endo
Micro
% cells / dataset

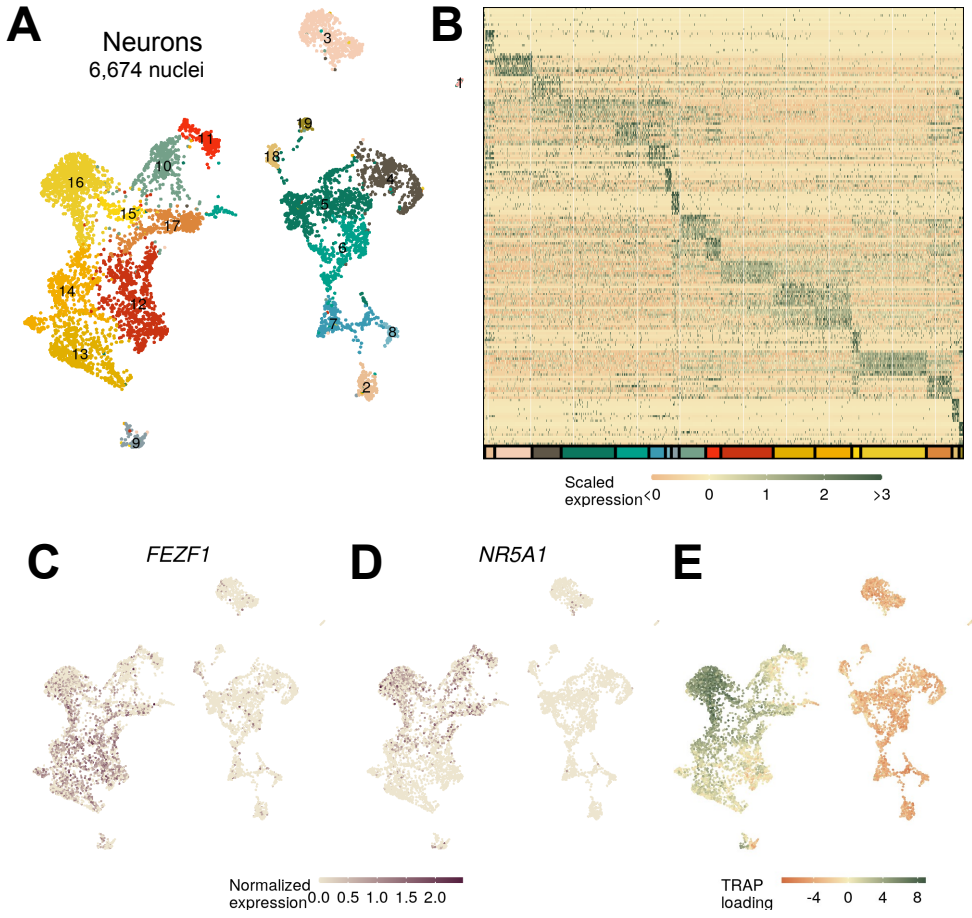
A
Neurons
6,674 nuclei
3
19
18
11
10
16
15
17
5
6
14
12
13
7
8
2
9
B
Scaled expression
<0
0
1
2
>3
C
FEZF1
Normalized expression
0.0 0.5 1.0 1.5 2.0
D
NR5A1
E
TRAP loading
-4 0 4 8

A

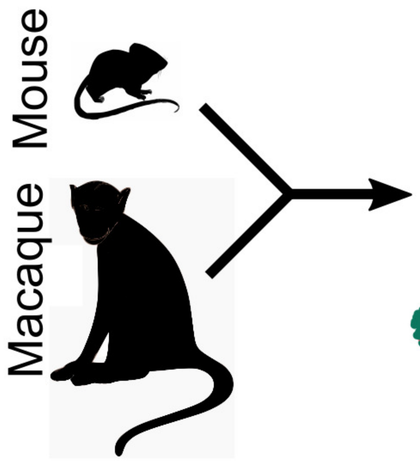
Mouse
Macaque

B


Macaque
Mouse

C

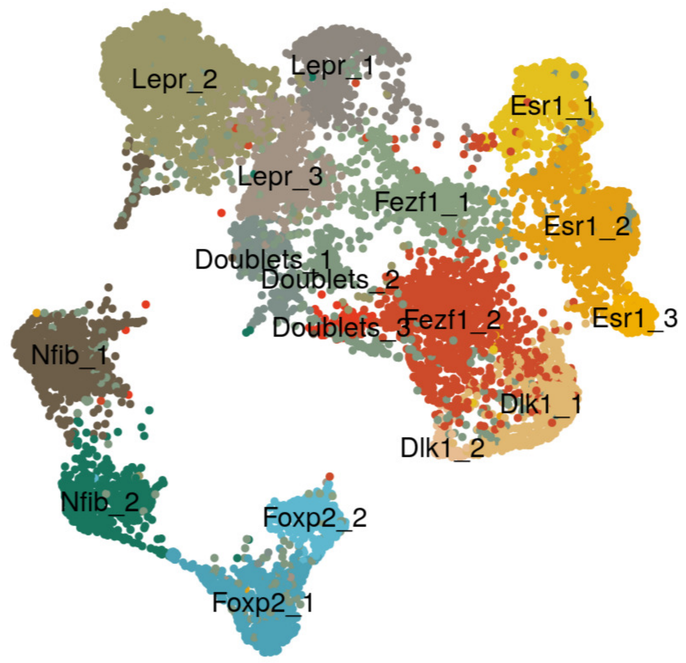
Lepr_2
Lepr_1
Esr1_1
Lepr_3
Fezf1_1
Esr1_2
Doublets_1
Doublets_2
Doublets_3
Fezf1_2
Esr1_3
Nfib_1
Dlk1_1
Dlk1_2
Nfib_2
Foxp2_2
Foxp2_1

D

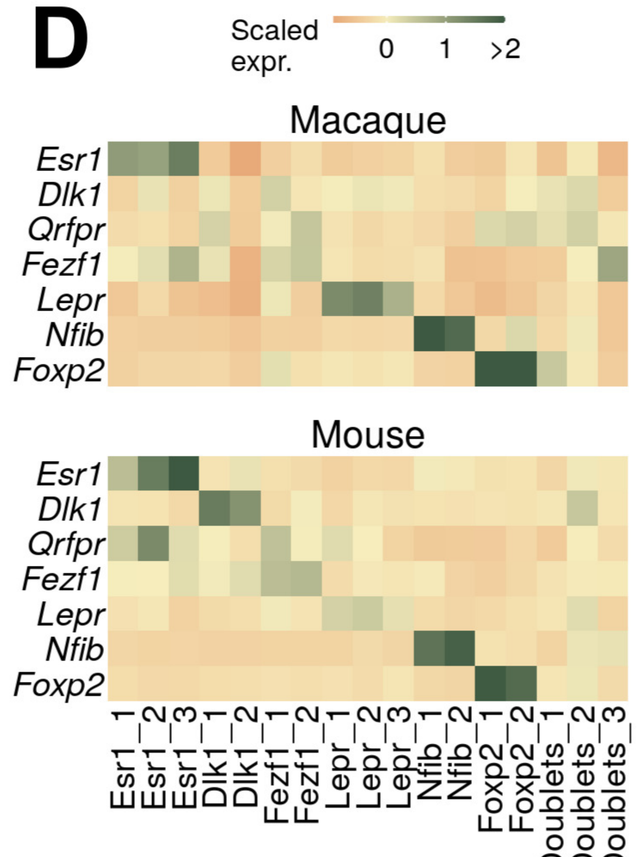
Scaled expr.
0
1
>2
Macaque
Esr1
Dlk1
Qrfpr
Fezf1
Lepr
Nfib
Foxp2
Mouse
Esr1
Dlk1
Qrfpr
Fezf1
Lepr
Nfib
Foxp2
Esr1_1
Esr1_2
Esr1_3
Dlk1_1
Dlk1_2
Fezf1_1
Fezf1_2
Lepr_1
Lepr_2
Lepr_3
Nfib_1
Nfib_2
Foxp2_1
Foxp2_2
oublets_1
oublets_2
oublets_3

E

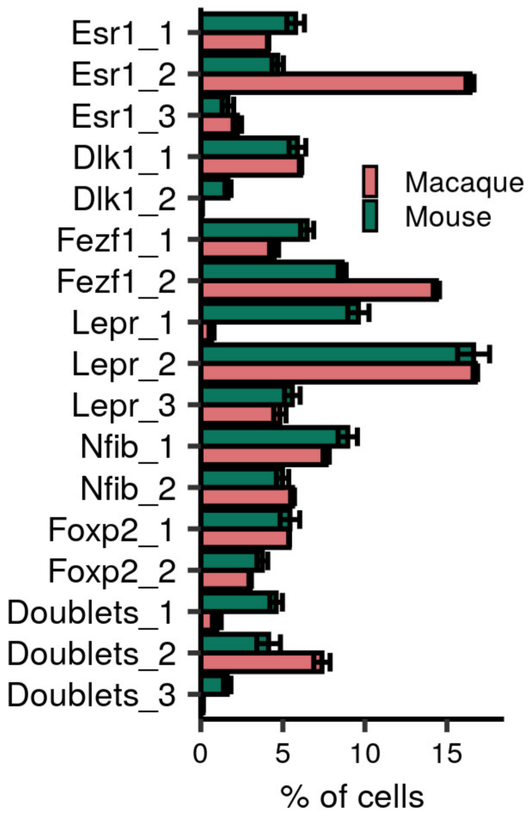
Esr1_1
Esr1_2
Esr1_3
Dlk1_1
Dlk1_2
Fezf1_1
Fezf1_2
Lepr_1
Lepr_2
Lepr_3
Nfib_1
Nfib_2
Foxp2_1
Foxp2_2
Doublets_1
Doublets_2
Doublets_3
Macaque
Mouse
0
5
10
15
% of cells

F

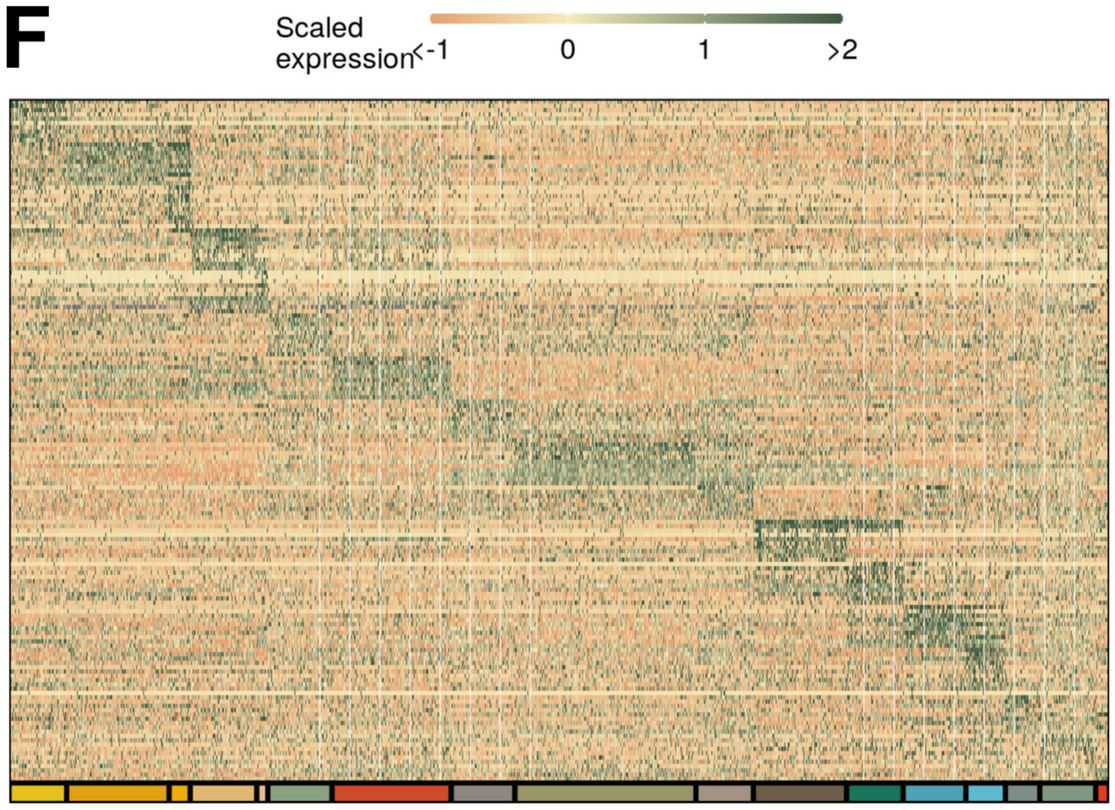
Scaled expression
<-1
0
1
>2

G

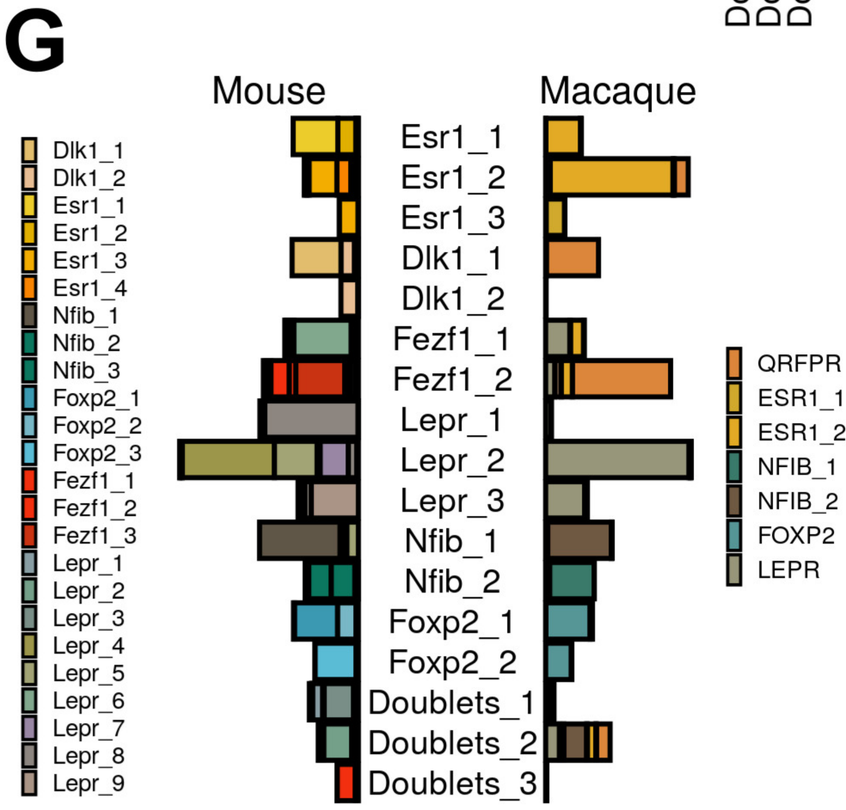
Mouse
Macaque
Dlk1_1
Dlk1_2
Esr1_1
Esr1_2
Esr1_3
Esr1_4
Nfib_1
Nfib_2
Nfib_3
Foxp2_1
Foxp2_2
Foxp2_3
Fezf1_1
Fezf1_2
Fezf1_3
Lepr_1
Lepr_2
Lepr_3
Lepr_4
Lepr_5
Lepr_6
Lepr_7
Lepr_8
Lepr_9
Esr1_1
Esr1_2
Esr1_3
Dlk1_1
Dlk1_2
Fezf1_1
Fezf1_2
Lepr_1
Lepr_2
Lepr_3
Nfib_1
Nfib_2
Foxp2_1
Foxp2_2
Doublets_1
Doublets_2
Doublets_3
QRFPR
ESR1_1
ESR1_2
NFIB_1
NFIB_2
FOXP2
LEPR

H

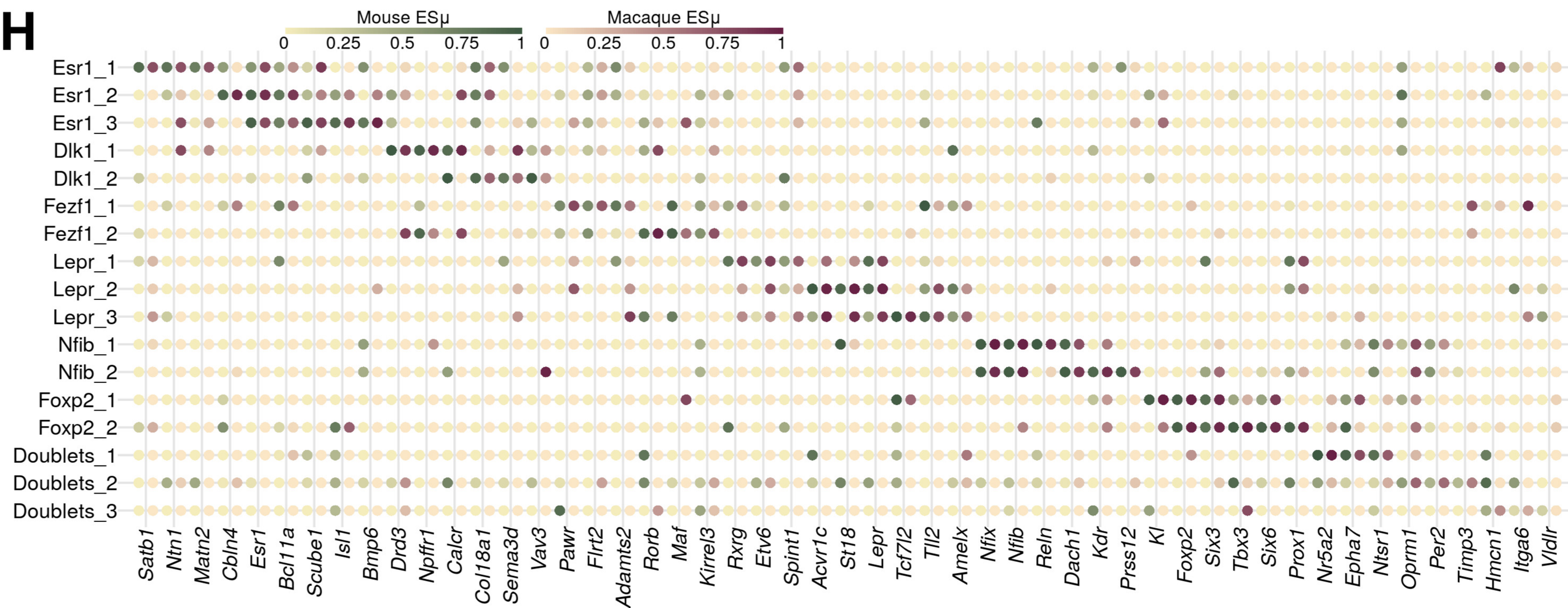
Mouse ESμ
0
0.25
0.5
0.75
1
Macaque ESμ
0
0.25
0.5
0.75
1
Esr1_1
Esr1_2
Esr1_3
Dlk1_1
Dlk1_2
Fezf1_1
Fezf1_2
Lepr_1
Lepr_2
Lepr_3
Nfib_1
Nfib_2
Foxp2_1
Foxp2_2
Doublets_1
Doublets_2
Doublets_3
Satb1
Ntn1
Matn2
Cbln4
Esr1
Bcl11a
Scube1
Isl1
Bmp6
Drd3
Npffr1
Calcr
Col18a1
Sema3d
Vav3
Pawr
Flrt2
Adamts2
Rorb
Maf
Kirrel3
Rxrg
Etv6
Spint1
Acvr1c
St18
Lepr
Tcf7l2
Tll2
Amelx
Nfix
Nfib
Reln
Dach1
Kdr
Prss12
Kl
Foxp2
Six3
Tbx3
Six6
Prox1
Nr5a2
Epha7
Ntsr1
Oprm1
Per2
Timp3
Hmcn1
Itga6
Vldlr

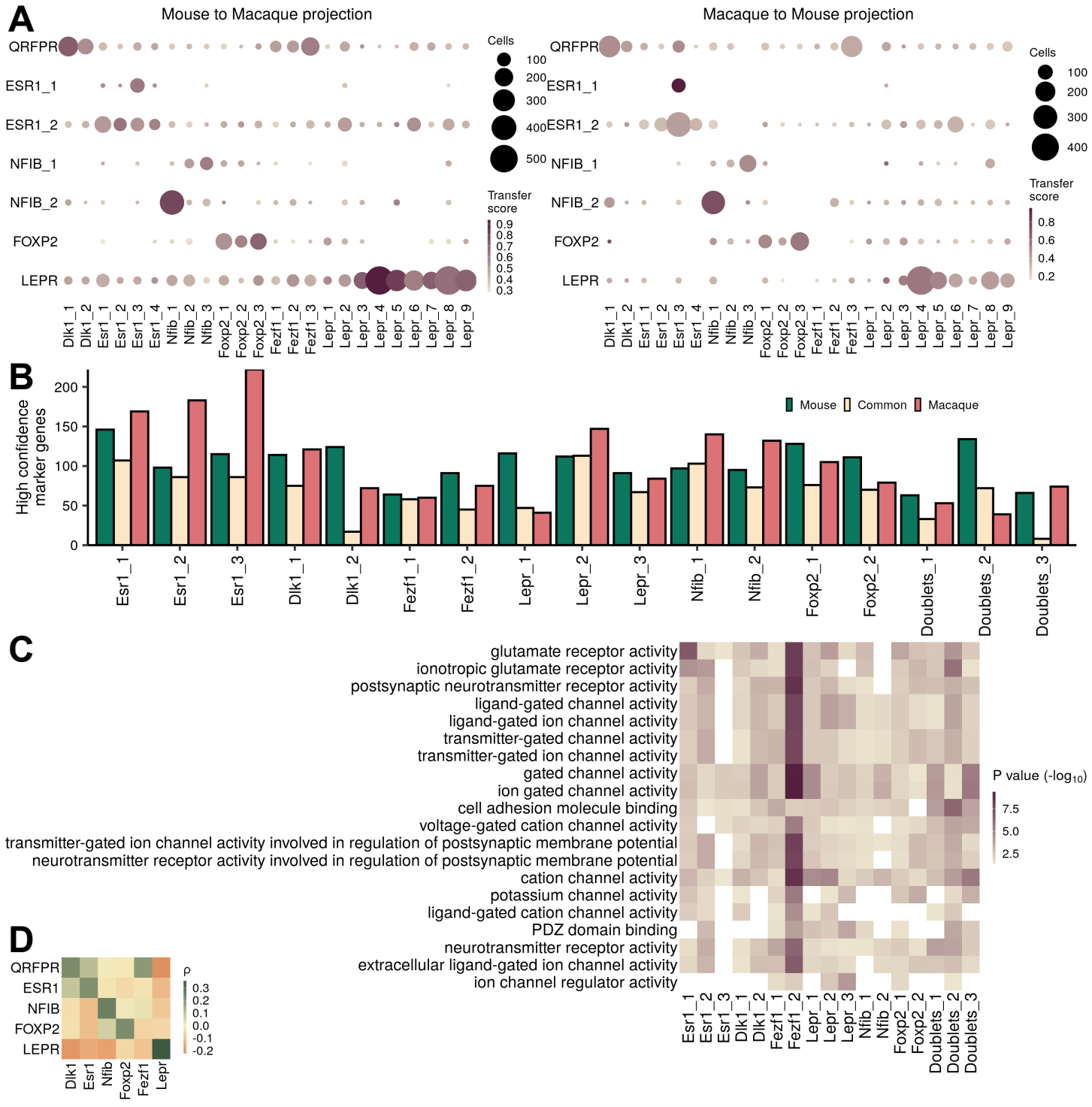
A
Mouse to Macaque projection
Macaque to Mouse projection
QRFPR
ESR1_1
ESR1_2
NFIB_1
NFIB_2
FOXP2
LEPR
Cells
Transfer score
Dlk1_1 Dlk1_2 Esr1_1 Esr1_2 Esr1_3 Esr1_4 Nfib_1 Nfib_2 Nfib_3 Foxp2_1 Foxp2_2 Foxp2_3 Fezf1_1 Fezf1_2 Fezf1_3 Lepr_1 Lepr_2 Lepr_3 Lepr_4 Lepr_5 Lepr_6 Lepr_7 Lepr_8 Lepr_9
B
High confidence marker genes
Mouse
Common
Macaque
Esr1_1 Esr1_2 Esr1_3 Dlk1_1 Dlk1_2 Fezf1_1 Fezf1_2 Lepr_1 Lepr_2 Lepr_3 Nfib_1 Nfib_2 Foxp2_1 Foxp2_2 Doublets_1 Doublets_2 Doublets_3
C
glutamate receptor activity
ionotropic glutamate receptor activity
postsynaptic neurotransmitter receptor activity
ligand-gated channel activity
ligand-gated ion channel activity
transmitter-gated channel activity
transmitter-gated ion channel activity
gated channel activity
ion gated channel activity
cell adhesion molecule binding
voltage-gated cation channel activity
transmitter-gated ion channel activity involved in regulation of postsynaptic membrane potential
neurotransmitter receptor activity involved in regulation of postsynaptic membrane potential
cation channel activity
potassium channel activity
ligand-gated cation channel activity
PDZ domain binding
neurotransmitter receptor activity
extracellular ligand-gated ion channel activity
ion channel regulator activity
P value (-log10)
D
QRFPR
ESR1
NFIB
FOXP2
LEPR
Dlk1 Esr1 Nfib Foxp2 Fezf1 Lepr
ρ

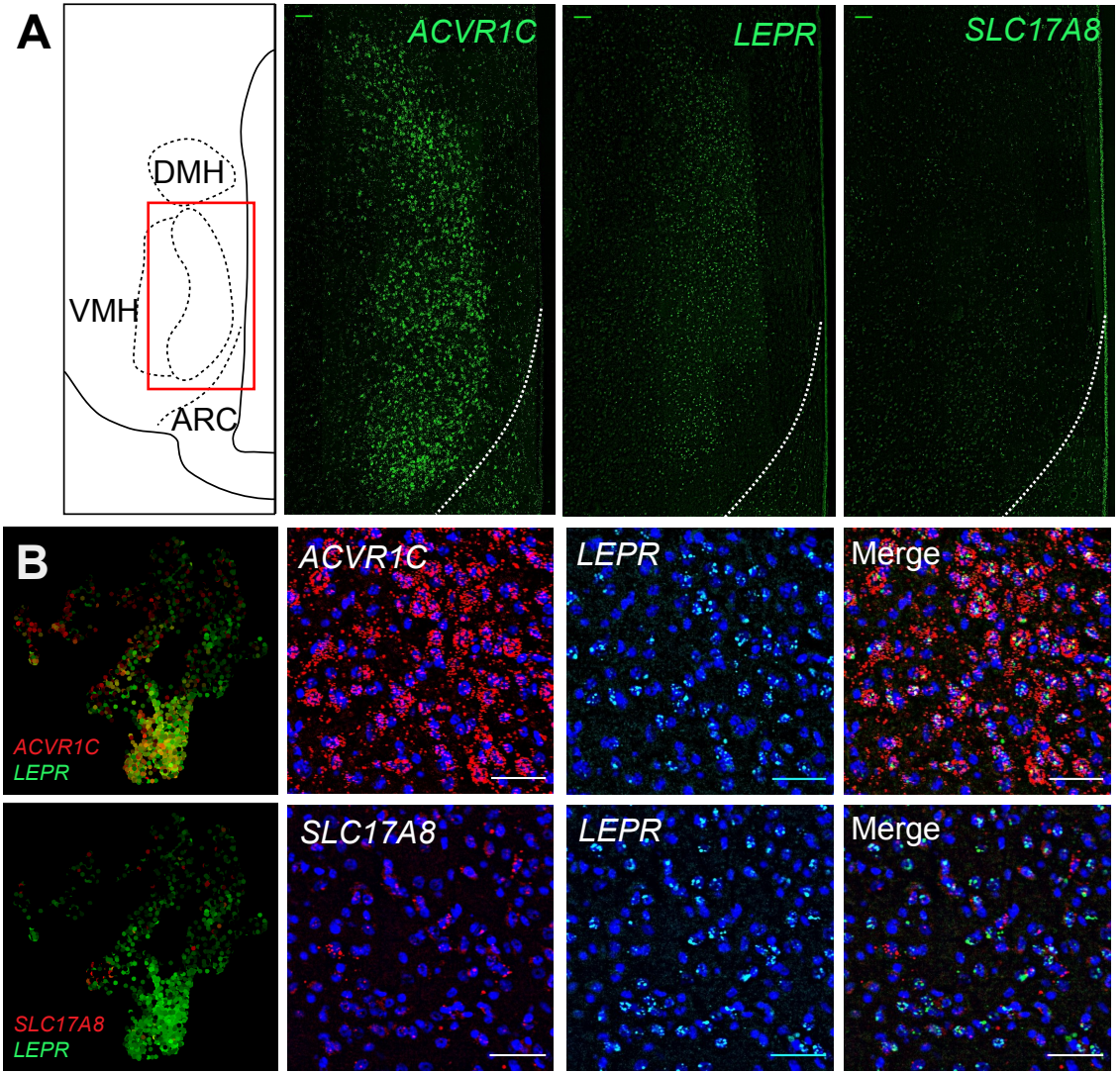
A
DMH
VMH
ARC
ACVR1C
LEPR
SLC17A8
B
ACVR1C
LEPR
Merge
ACVR1C
LEPR
SLC17A8
LEPR
Merge
SLC17A8
LEPR